Mathematical Model for Fines-Migration-Assisted Waterflooding With Induced Formation Damage

Abbas Zeinijahromi, Thi Kim Phuong Nguyen, and **Pavel Bedrikovetsky,** University of Adelaide

Summary

Permeability decline during corefloods with varying water composition, especially with low-salinity water, has been widely reported in the literature. This effect can provide a relatively simple method for mobility control during waterflooding.

In this work, new basic equations for waterflooding with salinity variations causing the detachment of fine particles, their migration, and their straining are derived. The maximum concentration of attached fine particles as a function of water salinity and saturation is used to model the fines detachment. In large-scale approximation, the equivalence between the model for two-phase flow with fines migration and the adsorption-free polymer-flood model is established, which allows applying a commercial polymer flood simulator for modeling the waterflood with induced fines migration. The modeling showed that the permeability decline in the water-swept zone, caused by the alteration of the injected water composition and induced fines migration, may be able to improve waterflood performance by delaying water breakthrough, increasing sweep efficiency, and reducing the water cut, thus providing a relatively simple method for mobility control during waterflooding.

Introduction

Mobilization of fines with permeability decline caused by decreased water salinity, increased flow velocity, and altered water pH or temperature, has been widely reported in the literature (Mungan 1965; Bernard 1967; Lever and Dawe 1984; Valdya and Fogler 1992; Khilar and Fogler 1998; Civan 2010). The effect is usually attributed to the expansion of double electric layer between the fine particle and rock surface, weakening of the total grain-rock electrostatic attraction, and the consequent particle detachment by drag and lifting forces **(Fig. 1).** The detachment of fine particles leads to a slight increase in permeability, while the plugging of the small pores causes significant permeability decline.

In regard to two-phase flow, Muecke (1979) claimed that the damaging fines particles are water-wet; their migration and straining inside the water phase results in decrease of relative permeability for water **(Fig. 2).** On the basis of the laboratory studies and the well-productivity analysis, Liu and Civan (1996), Bennion and Thomas (2005), and Civan (2007) arrive at the same conclusions about the nature of permeability damage during two-phase flow of oil with low-salinity water in rocks.

The tests by Sarkar and Sharma (1990) show less permeability damage caused by low-salinity water flow at the presence of residual oil than that for flow at the absence of oil. The higher the water wetness, the larger the permeability reduction under the presence of residual oil. The permeability reduction during low-salinity coreflood under the presence of residual oil is almost negligible in oil-wet cores. This allows the authors to formulate the fine particle lifting from the water-wet fraction of the rock surface as a main mechanism of permeability damage during two-phase flow with low-salinity water.

This paper (SPE 144009) was accepted for presentation at the SPE European Formation Damage Conference and Exhibition, Noordwijk, the Netherlands, 7–10 June 2011, and revised for publication. Original manuscript received for review 1 September 2011. Revised manuscript received for review 6 June 2012. Paper peer approved 9 June 2012.

Usually, fines migration and size exclusion result in decline of well productivity and injectivity, leading to the traditional view that fines migration should be avoided. However, during waterflooding, an induced reduction in the effective permeability to water in the water-swept zone caused by fines migration may be used to provide mobility control for improved performance of the waterflood. This effect is similar to that of other enhanced-oil-recovery mobility-control techniques such as polymer flooding. Reducing the salinity of the injected water appears to be the most practical method of implementing mobility control by induced fines migration, because other parameters controlling the release of fines (pH, temperature, and velocity) are not easily altered.

In this paper, the feasibility of using this effect of the water-phase permeability reduction for mobility control during low-salinity waterflooding is investigated.

Hussein et al. (2012) aimed to confirm these effects of the water-phase permeability reduction during high- and low-salinity waterflooding in oil-saturated rock. The Berea core was cut into three pieces. First, the potential for an intensive fine-particle release by freshwater injection was checked—the flooding of the first piece by water with decreasing salinity causes high permeability decrease and an intensive fines production. Then, the high- and low-salinity waterfloodings have been compared for the oil-saturated second piece. It was first saturated by oil at the presence of connate high-salinity water, with further displacement by the same high-salinity water. Afterward, it was resaturated by oil in the presence of connate high-salinity water with the following low-salinity water injection. The observed decrease in the relative permeability for low-salinity water, if compared with that for high-salinity water, was explained by lifting and straining of fines in the water-filled fraction of the porous space. Some decrease in residual oil after the low-salinity water injection was attributed to redirection of water into oil-filled pores by plugging of the water-saturated pores by migrating fines. Finally, it was concluded that the water-wet particles have been removed from the rock by moving low-salinity water, resulting in a decrease in relative permeability for water and in increase in fractional flow for oil. The conclusions agree with the mechanisms proposed by Muecke (1979) and Sarkar and Sharma (1990). Yet only phase rates and pressure have been measured during the tests. Measurements of effluent salinity and fines concentration, microscope photos, and mineralogical analysis of the produced fines would improve the quality of the analysis.

Recent investigations of low-salinity waterflooding have largely focused on the effects of water compositions on wettability, relative permeability, capillary pressure, and residual oil saturation (Tang and Morrow 1999; Yildiz and Morrow 1996; Pu et al. 2010; Jerauld et al. 2008; Takahashi and Kovcsek 2010; Berg et al. 2010; Cense et al. 2011; Mahani et al. 2011). Zhang and Morrow (2006) and Morrow and Buckley (2011) suggest also that the formation of lamellae and emulsions, stabilized by fines, their migration, and straining, may result in mobility control and redirecting the water flux. Tang and Morrow (1999) and Fogden et al. (2011) suggested another mechanism of oil-wet and mixed-wet fines detachment by advancing water/oil capillary menisci; the resulting straining may also decrease the water relative permeability and increase oil recovery. These effects appear to be separate phenomena from the fines lifted by low-salinity water and plugging of

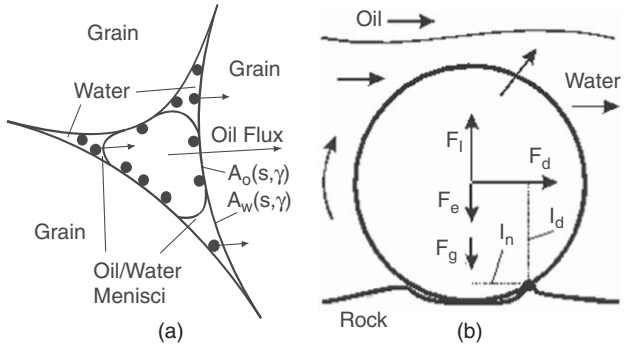

Fig. 1—Forces exerted on the attached fine particle during flow in porous media (torque balance on a single particle): (a) Fine particles attached to water-wet and oil-wet surfaces; (b) torques on a fine submerged in water.

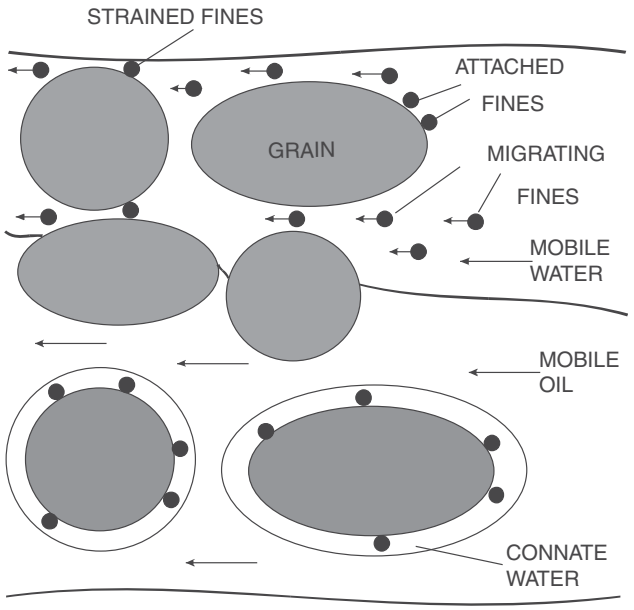

Fig. 2—Straining of detached particles in water-filled thin pores.

water-filled pores, but may occur simultaneously with fines migration. Some low-salinity coreflood studies have reported the release of significant amounts of fines (Bernard 1967; Tang and Morrow 1999; Pu et al. 2010), while others showed no evidence of fines migration (Lager et al. 2008; Jerauld et al. 2008; Rivet et al. 2010) even though additional oil was recovered. In order to separate these effects, the injections leading to fines lifting and permeability decline are described in the current work as "fines-assisted waterflooding."* The present paper only considers the effects of fines mobilization and capture to provide mobility control and does not consider changes to the residual oil saturation or relative permeability curves as a result of injecting low-salinity water.

The decision-making regarding the fines-assisted waterflooding (i.e., applying low salinity or high pH waters) is based on the results of laboratory-based mathematical modeling. Several models describing the release and capture of particles were developed. Microscale models of the particle capture include population balance equations (Sharma and Yortsos 1987a, b, c; Bedrikovetsky 2008) and trajectory analysis (Payatakes et al. 1973, 1974). Fine particle release is usually modeled by kinetics equations for the detachment rate that is assumed to be proportional to the difference between the current and critical values of the detaching factors, such as velocity, salinity, pH, shear, and temperature (Liu and Civan 1996; Tufenkji 2007; Ju et al. 2007; Rousseau et al. 2008; Yuan and Shapiro 2010; Civan 2010; Bradford et al. 2011a, b). The kinetics rate equations were found to exhibit a delayed response to an abrupt velocity rise or salinity decrease, which did not agree with the near-instantaneous response observed in laboratory experiments by Ochi and Vernoux (1998) and Bedrikovetsky et al. (2012). The alternative approach to the detachment modeling is the maximum attached fines concentration σ_{cr} as a function of the detaching factors U, γ, and T, which exhibit the core response without delay (Bedrikovetsky et al. 2011). Hence, the maximum retention function model for fines detachment $\sigma_{cr}(U, \gamma, T,\ldots)$, was chosen for derivation of fines migration equations in a two-phase environment in the current investigation.

The introduction of the maximum retention function allowed the effects of fines migration and permeability decline to be integrated into the quasi-2D Dietz model for waterflooding in a layer-cake reservoir (Lemon et al. 2011; Zeinijahromi et al. 2011). The Dietz model was used because it provided a relatively simple and transparent analytical solution. However, full separation of phases, assumed in the Dietz model, rarely occurs in real oilfields. Therefore, reservoir simulations of the fines-assisted waterflooding in real oilfields must be performed using 3D numerical models.

The current paper extends the previous works (Lemon et al. 2011; Zeinijahromi et al. 2011) to address 3D modeling of waterflood with fines migration.

The basic equations for two-phase flow with solute transport, fines lifting, and migration in aqueous phase with the following size exclusion are derived. The introduction of the maximum retention function for a two-phase environment allows the modeling of the fine-particle detachment; it integrates the effects of fines migration and permeability decline into the black-oil model for two-phase flow. The large-scale approximation of the governing system leads to an instant capture of released fines particles. The large-scale system can be represented in the form equivalent to that of the polymer-flooding model. The latter permits us to take advantage of the available polymer-flooding simulator for modeling of the low-salinity waterflood with induced migration of fines. The reservoir simulation of induced-fines-migration waterflooding is performed for heterogeneous formations. Two types of heterogeneity are considered: SPE-9 and five-layer-cake reservoirs. Injection of low salinity waterflooding with induced fines migration is found to be more effective for large scale heterogeneity with highly correlated flow paths, where it may result in significant sweep improvement.

The structure of the text is as follows. First, the maximum retention function as a model for fine particle detachment during two-phase flow is introduced. Then, the mechanism of mobility control improved oil recovery caused by induced fines migration and formation damage is presented. This is followed by the derivation of governing equations for a two-phase flow with salinity alteration, fine-particle mobilization, their migration in water, and straining. Then, the simplified model for large-scale approximation is presented. Next, the fines-assisted waterflood model in large-scale approximation is shown to be equivalent to the polymer-flooding model. The results of simulation of low-salinity waterflooding with fines mobilization and its comparison with normal waterflooding and polymer flooding conclude the paper.

Modeling Fines Release and Permeability Decline With Altered Injected-Water Chemistry

In this section, the maximum concentration of movable in-situ fines such as dispersed clay particles or mineral crystals attached to a rock surface as a function of water salinity and saturation is introduced in order to model the fine-particle detachment by flowing low-salinity water.

The classical filtration theory describes particle detachment with consequent migration and pore plugging for a single-phase flow. This model includes a mass-balance equation for particles with a sink term for particle retention and a source term for particle dislodging (Tufenkij 2007; Civan 2007, 2010; Bradford et al. 2011a, b). The kinetic relationships for particle detachment

* Personal communication, Kruijsdijk et al., Shell Research, 2011.

assume that the rate is proportional to the differences between the detaching factors (velocity, salinity, pH, and shear) and their critical values (Tufenkji 2007; Yuan and Shapiro 2010; Bradford et al. 2011a, b); here, the critical values correspond to mobilization of the "first" particle [see Miranda and Underdown (1993) and Khilar and Fogler (1998) for theoretical definition and laboratory determination of the critical values). Particle retention, represented by the filtration coefficient, is described by a rigorous theory that considers particle/grain and particle/particle interactions, flow velocity, Brownian diffusion, and gravitational sedimentation (Nabzar et al. 1996; Chauveteau at al. 1998; Tufenkji and Elimelech 2003; Rousseau et al. 2008). On the contrary, the detachment-kinetics coefficients are empirical constants determined usually by turning to experimental data (Ju et al. 2007; Tufenkji 2007), a process that requires extensive laboratory studies. Another shortcoming of the advective/diffusive model with particle-detachment kinetics is the asymptotical stabilization of the retention concentration and permeability with time tending to infinity. It causes a delayed response to an abrupt change in fluid velocity or composition contradicting the near-instant response observed in the laboratory experiments (Ochi and Vernoux 1998; Khilar and Fogler 1998; Bedrikovetsky et al. 2012). The fines mobilization occurs with the breaking of the force or torque equilibriums on the micro scale (Bergendahl and Grasso 2000; Civan 2007; Bradford et al. 2011b). Nevertheless, the classical filtration model, including a recent advance with a migrating layer of attached particles (Li et al. 2006; Yuan and Shapiro 2010), does not reflect the mechanical equilibrium of a fine particle. The current two-phase models with particle release also use the kinetics expressions for the detachment rate (Liu and Civan 1996; Ju et al. 2007; Ju and Fan 2009; Sbai and Azaroual 2011).

The modified particle-detachment model (Appendix A) uses the maximum (critical) retention function $\sigma_{cr}(\varepsilon)$, (Eqs. A-15 through A-17) instead of a kinetics expression to describe the particle detachment rate (Bedrikovetsky et al. 2011). Here, σ is the attached fines concentration, σ_{cr} is its maximum value, and ε is the ratio between the detaching and attaching torques (so-called erosion number). In this model, the particle capture continues according to the classical deep-bed filtration theory until the concentration of retained particles reaches its maximum, determined by the static equilibrium of the forces exerting a fine particle. Changes to fluid velocity or composition may abruptly reduce the maximum retained concentration below the current critical retained concentration, causing the instantaneous release of the fine particles. To simplify the model, all particles are assumed to be spheres of equal radii and of the same material. Pores are represented by cylindrical tubes and are distributed by radius. These assumptions are significant and require the model to be matched to laboratory data before its use. However, the maximum retention function is a reference characteristic of the rock and fluid. Therefore, once it is matched to a specific set of data, the effects of changes to velocity or water composition can be investigated without the need for additional laboratory data.

It is assumed that fine particles can be mobilized by water phase (Figs.1a and 2). The main forces considered acting on a particle located at the surface of a pore or on the internal particle cake are drag, lifting, buoyancy, and a total electrostatic force (Khilar and Fogler 1998; Bergendahl and Grasso 2000; Bradford et al. 2011b; Bedrikovetsky et al. 2011). Drag and lifting forces are caused by the flow of fluid over a particle and act to detach the particle from the pore wall (Fig.1b). Both forces increase with increasing of the linear flow velocity, particle radius, and the fluid viscosity (see the explicit expressions in Eqs. A-1 and A-2). For small particles of low to moderate density, the buoyancy force is insignificant compared to the magnitude of the other forces; hence, it can often be ignored. The total electrostatic force describes the interaction of a particle and the pore wall at very small separations and is independent of fluid velocity. For the purposes of the model describing the fine particle lifting, the total electrostatic force is taken as the maximum value of the sum of the van der Waals, electrical double layer and Born forces as described by the Derjaguin, Landau, Verwey, and Overbeek (DLVO) theory (Derjaguin and Landau 1941; Israelachvili 2006) (see Eqs. A-4 and A-5). The van der Waals force depends primarily on the Hamaker constant and is largely independent of changes in water composition (Hunter 2001). However, the electrical double layer force does depend on water composition, specifically ionic strength and pH. Therefore, it is through the electrical double layer force that changes to absolute salinity that concentrations of all ions, temperature, and pH affect the force balance and the maximum retention concentration. Typically for clastic reservoir rocks, the total attractive electrostatic force decreases as the water salinity decreases because of expansion of the double electrical layer. The dependency on pH is usually more complicated. A limitation of this modeling approach is that, to be accurate, it must consider all significant forces acting on a particle. The previously described forces are considered to be the most significant, although other forces exist, such as non-DLVO surface forces (Khilar and Fogler 1998; Israelachvili 2006; Takahashi and Kovscek 2010).

Concentration of attached fine particles does not only depend on the absolute salinity but also on the specific ionic composition including the relative concentration of multivalent ions (Ligthelm et al. 2009). That idea is expressed by the so-called Scheuerman diagrams (Scheuerman and Bergersen 1990), which describe the thermodynamic stability for different types of clay as a function of single- and double-valent ions.

The static equilibrium of a particle is determined by the balance of torques from the forces shown in Fig. 1 (Freitas and Sharma 2001; Schembre and Kovscek 2005; Civan 2007; Takahashi and Kovcsek 2010).

$$F_d l_d + F_l l_n = (F_e + F_g) l_n. \quad \ldots\ldots\ldots\ldots\ldots\ldots (1)$$

The expressions for forces are presented in Appendix A.

The dimensionless erosion number is introduced as the ratio between the detaching and attaching torques at the absence of attached fine particles:

$$\varepsilon = \frac{F_d l_d + F_l l_n}{(F_e + F_g) l_n}, \quad \ldots\ldots\ldots\ldots\ldots\ldots\ldots (2)$$

where F_d, F_l, F_e, and F_g are drag, lifting, electrostatic, and gravitational forces, respectively; l_d and l_n are the corresponding levers for the drag and normal forces. A particle is released if the total attaching torque exceeds the total detaching torque (see Eq. 1). This may occur because of an increase in the drag and lifting forces (because of an increase in flow velocity) or because of a decrease in the electrostatic force (because of a decrease in the water salinity or other change in water composition). The maximum concentration of retained particles is a function of the erosion number for any porous media. The derivation of equation

$$\sigma = \sigma_{cr}(\varepsilon) \quad \ldots\ldots\ldots\ldots\ldots\ldots\ldots\ldots (3)$$

for an average cylindrical capillary of the porous medium is based on the torque force equilibrium (see Eqs. A-7 through A-15). Eq. 3 for size-distributed capillary is determined by averaging (see Eqs. A-16 and A-17).

Let us compare the particle detachment model (Eqs. 3, A-17) with laboratory test data. Mungan (1965) has performed coreflooding with stepwise salinity decrease. The Berea sandstone contained kaolinite and illite clays. The clay minerals were identified by X-ray diffraction. The test shows the significant permeability decline **(Fig. 3a)** and the appearance of the mobilized fines in the effluent production. During the NaCl salinity decrease from 30,000 to 1 ppm, the permeability declined from 190 to 25 md. Other parameters included the porosity of 0.20, injection velocity $U = 1.6446 \times 10^{-5}$ m/s, and average pore radius of 8 μm. Pores were log-normally distributed between 0.1–30 μm, with a standard deviation of 5 μm. The explicit formulae for calculation of maximum retention concentration for each pore size (Eqs. A-15 through A-17), based on the torque balance of attaching and

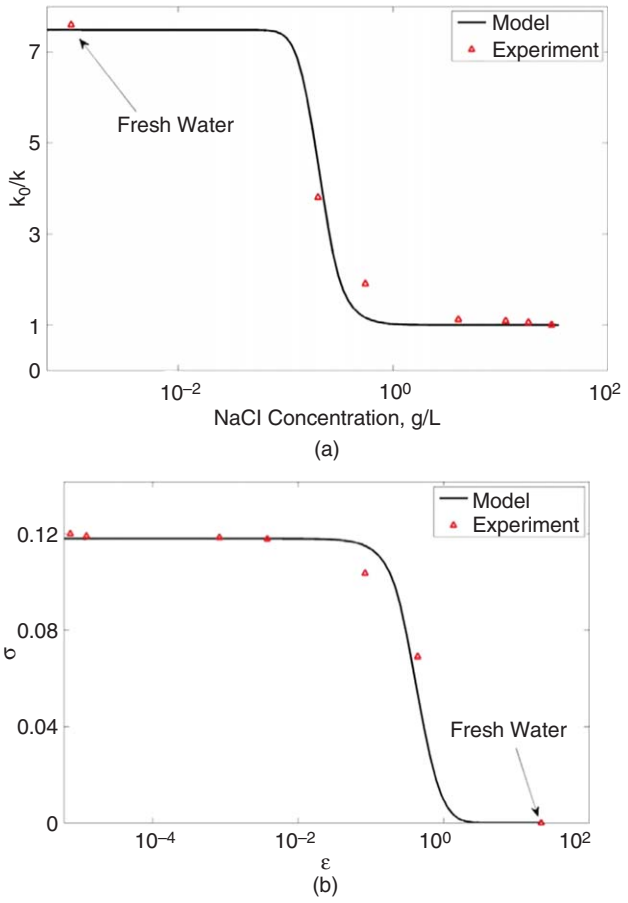

Fig. 3—Treatment of laboratory data by Mungan (1965): (a) decrease of permeability during waterflooding by water with piecewise decreasing salinity; (b) graph of the maximum retention function.

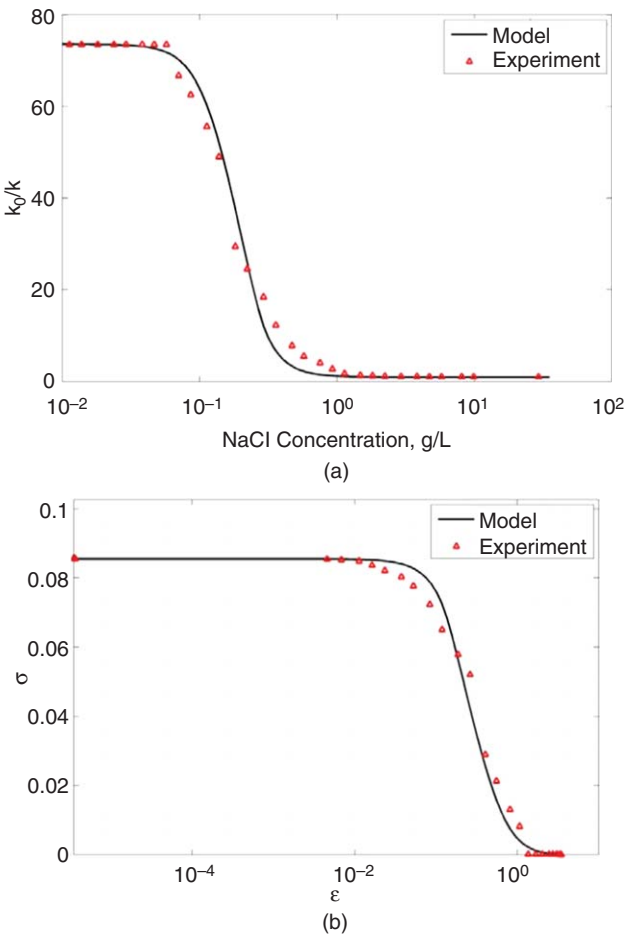

Fig. 4—Recovery of the maximum retention function from laboratory tests by Khilar (1983): (a) permeability vs. erosion number from coreflooding with piecewise decreasing salinity; (b) graph of the maximum retention function.

detaching forces, have been adopted. The Hamaker constant A_{132}, particle radius r_s, formation damage coefficient β and drag and lifting constants ω and χ have been chosen as tuning parameters. Minimization of the modeling data deviation from the laboratory data, using the standard ranges of the five parameters variation, gave the following: $A_{132}=1.3\times10^{-20}$ J, $r_s=0.3$ μm, $\beta=55$, $\omega=40$, and $\chi=48.8$. A good agreement between the experimental data and the micromodeling results (Fig. 3a for permeability decline, Fig. 3b for the maximum retention function) validates the theoretical concept of the maximum retention function (Eqs. 3 and A-15 through 17).

Khilar et al. (1983) has also performed corefloods with decreasing salinity of the injected water. The main observations also consisted of permeability decrease and the appearance of the released fine particles at the core outlet **(Fig. 4a).** The Berea sandstone contained 8% (w/w) of the dispersible kaolinite and illite clays. The outlet clay particle concentration was measured during the test. During the stepwise decrease in injected water ionic strength from 0.5 to 0.0002 M, permeability decreased by 73 times. The injection interstitial velocity was $U=7.126\times10^{-5}$ m/s. Other parameters used for the test included the porosity at 0.19 and the average pore radius at 10 μm. Pores were log-normally distributed between 0.1–50 μm, with a standard deviation of 10 μm. Minimization of the modeling data deviation from the laboratory data, using the standard ranges of the parameters variation, gave the following: $A_{132}=2.6\times10^{-20}$ J, $r_s=0.8$ μm, $\beta=850$, $\omega=10$, and $\chi=650$. Figs. 4a and 4b show a fairly good agreement between the laboratory data and the modeling-based prediction, which validates the proposed mathematical model for fine particle detachment, expressed by the maximum retention function.

The shape of the maximum retention function [$\sigma_{cr}(\varepsilon)$ in Figs 3 and 4] shows that the salinity required to release all mobile particles is greater than zero. This has significant practical implications because it demonstrates that not only fresh water can release of all the attached particles.

Fig. 5 shows the results of matching of the theoretical model (Eqs. A1 through A3) with the laboratory data on the sequential coreflood by water with the decreasing salinity (Lever and Dawe 1984).

The rock permeability decreased in a coreflood experiment with a natural sandstone core sample by water with decreasing salinity (Fig. 5a). The permeability continuously decreased from 140 to 12 md, with the decrease of water salinity from 30 g/L to essentially zero (distilled water). Because the concentration of strained particles is equal to the concentration of detached particles minus the concentration of particles produced at the core effluent, the curve of stabilized permeability vs. the salinity curve in Fig. 5 could be recalculated into the maximum retention function (Eqs. 1 through 3, Eqs. A-15 through A-17) (Fig. 5b). The following data were used for this transformation: flow velocity $U=10^{-6}$ m/s, $\beta=160$, Hamaker constant $A_{132}=0.8\times10^{-20}$ J, particle size = 1 μm, and drag and lifting factors $\omega=60$ and $\chi=649$, respectively. The log-normal pore-size distribution was assumed, where the mean (5 μm) and the standard deviation (5 μm) have been matched by permeability and porosity. Because flow velocity is unavailable from the original paper, the sensitivity with respect to flow velocity has been performed. All theoretical points as calculated by Eqs. A-15 through A-17 are located on the same maximum retention curve. Yet the experimental points corresponding to different velocities lay on the different curves $\sigma_{cr}(\varepsilon)$ (see blue, green, and red points in Fig. 5b). The curve $\sigma_{cr}(\varepsilon)$, as obtained for an average pore of the rock, was matched adequately with the experimental points for velocity $U=10^{-6}$ m/s.

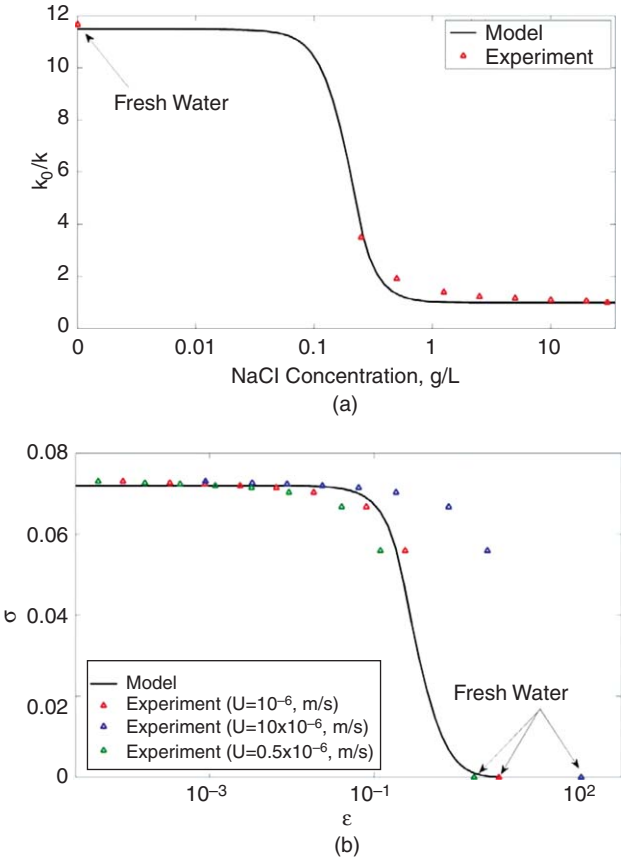

Fig. 5—Maximum retention function fitted to experimental data by Lever and Dawe (1984): (a) permeability decline with decrease of injected water salinity; (b) attached fines concentration vs. erosion ratio.

Fig. 5 shows a good agreement between the data of the coreflood with stepwise decreasing water salinity and the maximum retention in a single cylindrical capillary as obtained for different flow velocities. As more parameters have been controlled in the tests by Lever and Dawe (1984) compared with the two previous tests, the maximum retention function as matched by these experimental data will be used for reservoir simulations further in this paper.

Fine particle release during gradual water saturation increase is shown in Fig. 1a. It is assumed that the oil-wet and mixed-wet fines, attached to the rock surface accessible to mobile oil, cannot be detached by drag and lifting forces exerting from the mobile-oil phase. Water-wet particles are immersed in the connate water films and cannot be mobilized by the moving oil because it is assumed that the connate water cannot be mobilized (Fig. 2). The particles are released by detaching forces in mobile water. Arrival of low-salinity water weakens the attaching electrostatic force and the detaching forces entrain the fines. Therefore, the attached fines concentration remains the same in oil-filled pores. It is assumed that the detachment in water-filled pores is determined by torque balance and is described by the maximum retention function (Eqs. 1 through 3 and Eqs. A-15 through A-17):

$$\sigma_a(U_w,\gamma,s)=\frac{\sigma_{cr}(U_w,\gamma)A_w(s,\gamma)+\sigma_{a0}[A-A_w(s,\gamma)]}{A},$$
$$U_w=Uf(s,\sigma_s)\Big/s(\phi-\sigma_a-\sigma_s) \quad \ldots\ldots\ldots\ldots (4)$$

Here, U_w is an interstitial velocity of water. If compared with the maximum retention function for a single-phase flow (Eq. 3), the two-phase model for fine particle detachment (Eq. 4) accounts for saturation dependencies of water velocity (Yuan and Shapiro 2011) and of the rock surface fraction accessible to flowing water (Zeinijahromi et al. 2011b).

At the constant salinity, the fractions of the rock surface accessible to moving water and oil depend on saturation. Because wettability of rock changes with salinity decrease, these fractions of rock surface are also salinity-dependent. Therefore, the maximum retention concentration (Eq. 4) is also a function of saturation (Yuan and Shapiro 2011):

$$\sigma_a=\sigma_{cr}(\varepsilon,s). \quad \ldots\ldots\ldots\ldots\ldots\ldots\ldots\ldots (5)$$

Fig. 1a shows the fine particle release from the moving-water-exposed surface during gradual water saturation increase. The mobilized particles are initially water-wet fines or those with alternated wettability after the freshwater arrival (Berg et al. 2010, Cense et al. 2011).

Following Pang and Sharma (1997), Bedrikovetsky et al. (2001), and Mojarad and Settari (2007), it is assumed that the inverse of the normalized permeability $k\ (\sigma)/k_0$ is a linear function of the retained particle concentration:

$$\frac{k_0}{k(\sigma)}=1+\beta\sigma, \quad \ldots\ldots\ldots\ldots\ldots\ldots\ldots\ldots (6)$$

where β is the so-called formation damage coefficient. Eq. 6 corresponds to first-order Tailor's expansion of monotonically increasing function on the left side of the equation. More complex dependencies include second-order expansion or using the exponent on the left side of Eq. 6, yet those contain more empirical constants that must be determined from laboratory data. The formation damage coefficient for straining is assumed to be much greater than that for attachment [i.e., the detachment of fines causes a negligibly small permeability increase, while the plugging of pore throats results in a significant decrease in permeability (Fig. 1b)]. Therefore, σ in Eq. 6 corresponds to the concentration of strained particles.

Later in the text, the maximum retention function (Eqs. 4 and 5) will be used to model fines detachment and the formation-damage function (Eq. 6) will be applied in the modified Darcy's law to describe a decrease in water relative permeability caused by straining of the mobilized fines.

Mechanism for Improved Sweep Efficiency Caused by Fines Migration

These observations—that fines migration can cause permeability decline because of changes in water composition (Eqs. 4 through 6)—are sufficient to warrant the consideration of the effects of induced fines migration on waterflooding. During a waterflood, the rapid breakthrough of water can be a significant problem, leading to high water cut at producing wells and lower volumetric sweep efficiency. The problem is particularly pronounced for a mobility ratio significantly greater than unity or where the variation of permeability across the reservoir is significant. Mobility-control techniques, such as polymer flooding, may be employed to reduce a high mobility ratio by increasing the viscosity of the injection water or decreasing the effective permeability to water of the reservoir in the water-swept zone behind the flood front (Lake 1989). Such techniques decrease the fractional flow of water in the reservoir and thus decrease the water cut at the producing wells. The volumetric sweep efficiency is also improved. Fines release, caused by the alteration of the chemistry of the injected water, and the consequent decrease in permeability, may be able to provide the mobility control and hence the ability to improve waterflood performance (Zhang and Morrow 2006; Lemon et al. 2011; Zeinijahromi et al. 2011). Because the mobilization of fines by changing the chemistry of the injected water can only take place in the water-swept zone, only the effective permeability to water of the reservoir is decreased, reducing the mobility ratio. However, the main disadvantage of mobility control is that, for a given injection rate, the induced formation damage results in an increased injection pressure.

Fig. 6 shows the lateral displacement of oil by water in a heterogeneous reservoir with low-permeability zones adjacent to the

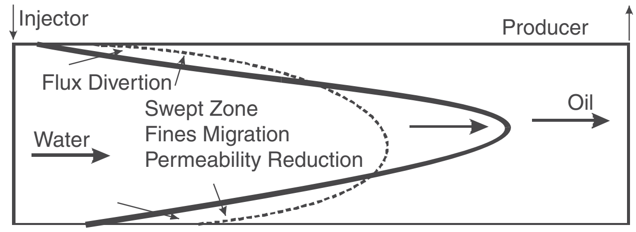

Fig. 6—Schematic for incremental sweep efficiency by induced fines migration.

reservoir top and bottom, and high permeability in the central layers. In the thin reservoir under consideration, the gravity effects are negligible. The continuous curve corresponds to the displacement front under normal waterflooding. Water propagates preferentially in the highly permeable central zones, with slow displacement of the oil in low-permeability zones near to the reservoir top and bottom. A further slowing of the displacement front in the low-permeability zone occurs after water breakthrough in central highly permeable zones and the creation of an injector/producer channel filled by high-mobility water. The formation damage induced by mobilized fines in the swept zone tends to homogenize the permeability distribution across the reservoir (see the dashed curve in Fig. 6) and diverts the injected water into unswept areas. Hence, the induced formation damage causes the delayed breakthrough period and improved sweep efficiency for a given volume of injected water.

In the next section, the mathematical model describing the improved sweep efficiency caused by fines migration and size exclusion is derived.

Basic Equations for Fines Migration Under Two-Phase Flow

Let us discuss a system of two-phase flow in porous media with varying water salinity, resulting in the fine particles lifting. Following Muecke (1979), it is assumed that the water-wet particles are transported by the water phase (Fig. 2). The detached forces mobilize water-wet fines that have been water-wet originally or, according to Berg et al. (2010) and Cense et al. (2011), became water-wet after the arrival of low-salinity water; the mobilization occurs if the detaching torque of drag and lifting forces exceeds the attaching torque of electrostatic and gravity forces (Eq. 1). It is assumed that the detached fines are inert (i.e., they are intact and keep their integrity during detachment). The effects of clay swelling are assumed to be negligible. For simplicity, we assume that the volumetric concentrations of attached and retained particles are negligibly small comparing to the porous space (i.e., the retention of fine particles does not affect the porosity). It is assumed that the initial salt concentration is the critical salt concentration for the reservoir fines, $\sigma_{a0}=\sigma_{cr}(\gamma_i)$ (i.e., the reservoir fines start leaving the rock surface with the decrease of salt concentration starting from $\gamma=\gamma_i$). We also assume that the dissipation effects of diffusion and capillary pressure are negligibly smaller than those of fines straining. Alteration of water salinity affects the attached concentration more strongly than does the velocity alteration; therefore, the velocity dependency of the maximum concentration of attached fines is neglected (Eq. 4). The permeability damage by fines straining is significantly higher than that caused by attachment. Other assumptions include constant temperature, incompressibility of water and oil, and constant water and oil viscosities.

Volumetric balance of the overall flux of incompressible water and oil is

$$\nabla\vec{U}=0. \quad (7)$$

Volumetric balance for incompressible water is (Lake 1989)

$$\phi\frac{\partial s}{\partial t}+U\nabla f(s,\sigma_s)=0, \quad (8)$$

where the fractional flow function accounts for the reduction of relative phase permeability for water according to Eq. 6:

$$f(s,\sigma_s)=\left[1+\frac{k_{ro}(s)\mu_w(1+\beta\sigma_s)}{k_{rw}(s)\mu_o}\right]^{-1} \quad (9)$$

and $\vec{U}$ is a 3D vector of the overall water-oil flux:

$$\vec{U}=(u_x,u_y,u_z).$$

The mass balance of suspended, attached, and retained particles is

$$\frac{\partial}{\partial t}[\phi sc+\sigma_a+\sigma_s]+U\vec{\nabla}(cf)=0. \quad (10)$$

Here it is assumed that no fine-particle attachment occurs in the reservoir during the injection of water without fines. Particle detachment occurs during injection of low-salinity water into the oil field, where the attached fines with maximum concentration are in contact with water with continuously decreasing salinity [i.e., the attached concentration is determined by the maximum retention function (Eq. 4), where drag and lifting forces are determined by interstitial velocity of water (Yuan and Shapiro 2011)]. Eq. 4 means an instant particle release governed by the torque balance.

Size-exclusion capture of mobilized fine particles in small pores is described by the equation of the linear kinetics (Bedrikovetsky 2008):

$$\frac{\partial\sigma_s}{\partial t}=\lambda_s cUf. \quad (11)$$

Here, the straining rate is proportional to water flux $f(s)U$ because the mobilized fine particles are transported by the water phase.

The mass balance of salt in the aqueous phase assumes low salt concentration not affecting the aqueous phase density ρ_w:

$$\frac{\partial}{\partial t}[\phi\gamma]+\vec{\nabla}(\gamma\vec{U})=0. \quad (12)$$

The modified Darcy's law for two-phase flow accounting for permeability damage to water is

$$U=-k\left[\frac{k_{rw}(s)}{\mu_w(1+\beta\sigma_s)}+\frac{k_{ro}(s)}{\mu_o}\right]\nabla p. \quad (13)$$

The important difference between the particle release under one phase and two-phase flows is the saturation dependency of the maximum retention function. It reflects the fine-particle release from the rock surface exposed to moving water only.

Finally, the system of governing equations for two-phase oil/water flow with fines mobilization, caused by the decrease in water salinity and the consequent reduction of relative permeability for water, consists of seven equations:

- Volumetric balance for incompressible flux of carrier water and oil
- Volumetric balance for incompressible water
- Mass balance for suspended, attached, and strained particles
- Maximum concentration of attached fine particles as a function of interstitial water velocity, salinity, and saturation
- Size-exclusion retention rate
- Advective mass transfer of salt in porous space with retained fines
- Modified Darcy's law accounting for permeability reduction caused by fines straining

These represent Eqs. 7, 8, 10, 4, and 11 through 13, respectively. This system determines seven unknowns: σ_a, s, p, c, γ, σ_s, and U.

The initial conditions corresponding to injection of low salinity water into an oil-bearing formation include initial water saturation and initial concentrations of salt and of attached particles, zero values of suspended and strained fines. Boundary conditions on the injection wells include rate, unit fractional flow for water,

salt concentration, and zero concentration of suspended fines. Well bottomhole pressure is a boundary condition at the production wells. The dimensionless form of the governing equations is presented in Appendix B.

The previously described system describes fines-assisted waterflooding for all length scales, from core to a reservoir. Yet, as is shown in the next section, the system can be significantly simplified at the reservoir scale.

Large-Scale Approximation

Let us derive the asymptotical form of the system (Eqs. B-2 through B-8) of oil/water flow in porous media with fines migration for large reservoir scale. The distance that the fine particle travels before being strained (the free run length of the particle) during deep-bed filtration is equal to the reciprocal filtration coefficient (Sharma and Yortsos 1987a, b, c; Nabzar et al. 1996; Chauveteau et al. 1998). In large scale, the particle free run is negligible if compared with the reservoir length:

$$\frac{1}{\lambda_s} \ll L$$

i.e., the dimensionless filtration coefficient for straining:

$$\lambda_s L \gg 1. \quad \ldots\ldots\ldots\ldots\ldots\ldots\ldots\ldots\ldots\ldots (14)$$

Tending $\lambda_s L$ to infinity on the left side of Eq. B-4 under limited retention rate and flow velocity results in the dimensionless suspended concentration tending to zero. Thus, ignoring the suspended concentration in Eq. B-4 yields

$$\frac{\partial}{\partial t}(S_a + S_s) = 0$$

i.e.,

$$S_s = 1 - S_a(\varepsilon, s). \quad \ldots\ldots\ldots\ldots\ldots\ldots\ldots\ldots\ldots\ldots (15)$$

Eq. 15 means that in large-scale approximation, where the free particle run length is negligible if compared with the inter-well distance, the lifted fines are immediately captured by size exclusion in porous media. The amount of strained fine particles becomes equal to the amount of mobilized fines.

Accounting for Eq. 15, the system of governing equations (Eqs. 7, 8, 10, 4, and 11 through 13) is transformed to the following equations for the total volumetric balance for water and oil:

$$\nabla(u) = 0 \quad \ldots\ldots\ldots\ldots\ldots\ldots\ldots\ldots\ldots\ldots (16)$$

of volume balance for water

$$\frac{\partial s}{\partial t_D} + u\nabla f\Big(s, 1 - S_a(\varepsilon, s)\Big) = 0 \quad \ldots\ldots\ldots\ldots\ldots (17)$$

where the fractional flow and maximum retention functions are

$$f\Big(s, 1 - S_a(\varepsilon, s)\Big) = \left[1 + \frac{k_{ro}(s)\mu_w\Big(1 + \beta\sigma_{a0}\Big(1 - S_a(\varepsilon, s)\Big)\Big)}{k_{rw}(s)\mu_o}\right]^{-1}$$

$$S_a = S_a(\varepsilon, s), \quad \varepsilon = \varepsilon\left(\gamma, {}^{Uf}\!/_{\phi s}\right)$$

of mass balance for salt is

$$\frac{\partial(\gamma s)}{\partial t_D} + u\nabla(\gamma f) = 0 \quad \ldots\ldots\ldots\ldots\ldots\ldots\ldots (18)$$

and the modified Darcy's law for two-phase flow and permeability damage in pores where water moves is

$$u = -\left[\frac{\mu_o k_{rw}(s)}{\mu_w\Big(1 + \beta\sigma_{a0}\Big(1 - S_a(\varepsilon, s)\Big)\Big)} + k_{ro}(s)\right]\nabla P. \quad \ldots (19)$$

The large-scale approximation system of four equations (Eqs. 15 through 19) describes low-salinity waterflooding with fines lifting, migration, capture, and subsequent permeability damage. The number of unknowns in this system is also reduced to four: saturation s, pressure P, salt concentration γ, and total velocity of two-phase flux u. The initial conditions include the initial values of water saturation, salt, and attached fines concentrations. Boundary conditions on injection wells include rate, unit fractional flow for water, and concentration of injected salt. Well bottomhole pressure is a boundary condition at production wells. The system in Eqs. 15 through 19 describes the fines-assisted waterflooding at large length reservoir scale, where the reference size highly exceeds the length of the free run of the fine particle. The laboratory-scale coreflood, where the core size has the same order of magnitude as the free run length, is described by the full system (Eqs. B-2 through B-8).

In the next section, we transform the model for water/oil flow with fines migration into the system of equations for polymer flooding, for which the reservoir simulator already exists.

Using Polymer Flooding Simulator For Modeling the Fines-Assisted Waterflooding

The system of governing equations (Eqs. 15 through 19) for fines-assisted waterflooding in a system of wells in heterogeneous reservoirs can be solved by numerical methods (Yuan and Shapiro 2011). The numerical code would be similar to that for chemical flooding. Yet if a reservoir simulator with an open source code is not available, already-existing commercial simulators for polymer flooding can be used for modeling of the fines-assisted waterflooding. It can be achieved by the mapping of the model for fines-assisted waterflooding onto equations for polymer flooding. Appendix C presents equivalence between the polymer-flooding model (Eqs. C-1 through C-6) and Eqs. 15 through 19. Here, Eq. C-8 expresses polymer concentration through water salinity; Eq. C-9 expresses the adsorbed polymer concentration through concentration of mobilized fines, and the expression for residual resistance factor is given by Eq. C-11.

Viscosity of the aqueous fines suspension with varying salinity is assumed to be constant and equal to water viscosity. Because the mass-balance equation for salt is mapped on the mass-balance equation for polymer, the viscosity of the polymer solution also becomes equal to constant water viscosity. Therefore, the only mobility control physics factor in the mapped polymer flood model is the resistance caused by polymer adsorption.

The mapping transforms (Eq. C-3) of mass balance for polymer accounts for adsorption in Eq. 18 of mass balance for salt without adsorption. Therefore, the expression in Eq. C-9 translating adsorbed polymer concentration in the concentration of released fines contains the small parameter δ. It allows neglecting salt adsorption but accounts for resistance factor caused by adsorbed polymer/strained fines (Eq. C-12).

Modeling Displacement in Homogeneous Five-Spot Pattern

The polymer injection black-oil model (Schlumberger 2010) was used to simulate the displacement of oil by water in five-spot pattern of a homogeneous one-layer reservoir. The adsorption isotherm was calculated using the formula in Eq. C-9 for the maximum retention function obtained from data of Lever and Dawe (1984) (Fig. 5). The residual resistance factor is assumed to be 10. The reservoir and fluid data are as follows: permeability 150 md, oil viscosity 50 cp, layer thickness 30 ft, size of the reservoir 2,500×2,500 ft, injection rate of 1,100 bbl/d, initial water saturation 0.15, residual oil saturation 0.12, $k_{rwor} = 0.49$, and $k_{rowr} = 0.9$, respectively. **Fig. 7** presents the areal saturation field for both scenarios. Fig. 7a shows the distribution of injected water and the oil displacement just after the breakthrough time for the normal

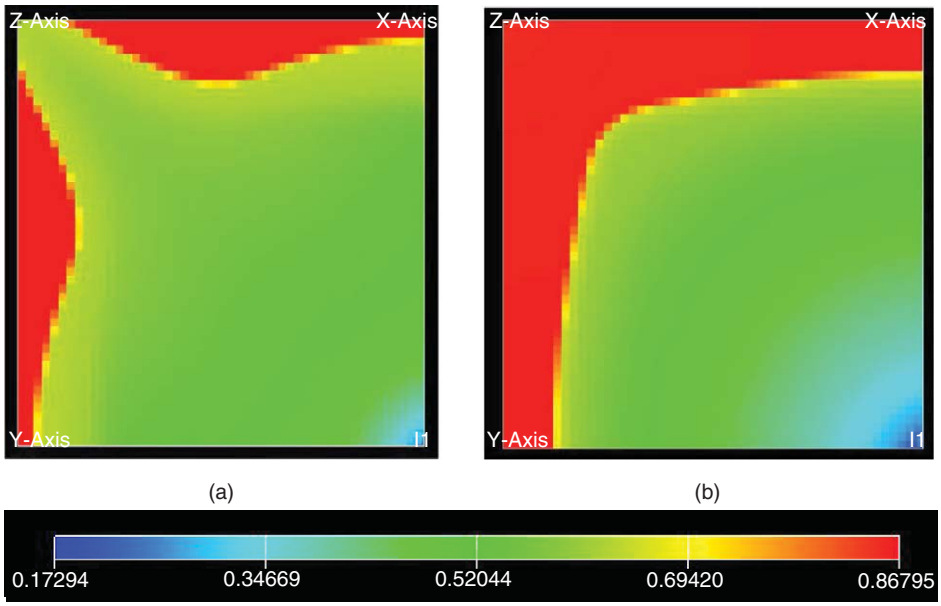

Fig. 7—Improved areal sweep in five-spot pattern during fines-assisted waterflooding before the breakthrough: (a) sweep for normal waterflooding; (b) saturation field for fines-assisted waterflooding.

waterflood, whereas the saturation distribution at the same moment after injection of low salinity water is shown in Fig. 7b. Injection of freshwater, mobilization of fines, consequential permeability decrease in swept zone, and slowdown of the displacing water results in the prolongation of the dry water-free production period.

The results of waterflooding after 1 PVI are shown in **Fig. 8.** Except of some neighborhoods around the injection well, oil saturation in the pattern varies around 0.64 during the normal waterflood (Fig. 8a) while during fresh waterflooding, most of the pattern area is saturated by oil and water with saturation of 0.44 (Fig. 8b). Therefore, the injection of fresh water results in significantly lower residual oil saturation. Consequently, the recovery factor for the case of freshwater injection (Figs. 7b, 8b) is higher than that for normal waterflooding (Figs. 7a, 8a).

Reservoir Simulation in Five-Layer-Cake 0Five-Spot Pattern

Let us discuss reservoir simulations of waterflooding using normal and fresh water in a five-spot pattern of a five-layer-cake reservoir **(Fig. 9a and b).** Values for permeability and thickness of the layers are presented in **Table 1,** with permeability increasing top down. The results are presented in Fig. 9 after injection of 0.6 PVI. The figure shows the top view of the high-permeability layer; the side and top views are presented for the quarter of the pattern for layers 1 through 4. The highly permeable layer at the moment of 0.6 PVI is completely swept in the case of freshwater injection (Fig. 9b), while a significant amount of residual oil remains in the highly permeable layer during normal waterflooding (Fig. 9a). The residual oil in the swept zone is significantly lower for fresh waterflood than it is for normal waterflood.

Comparison Between Normal Waterflood, Fines-Assisted Waterflooding, and Polymer Injection

In this section, the recovery during normal waterflood, fines-assisted waterflooding, and polymer injection are compared for the case of displacement in the five-spot pattern. Two cases of reservoir heterogeneity are discussed: the five-layer-cake reservoir and areal heterogeneity SPE-9 (Schlumberger 2010). First,

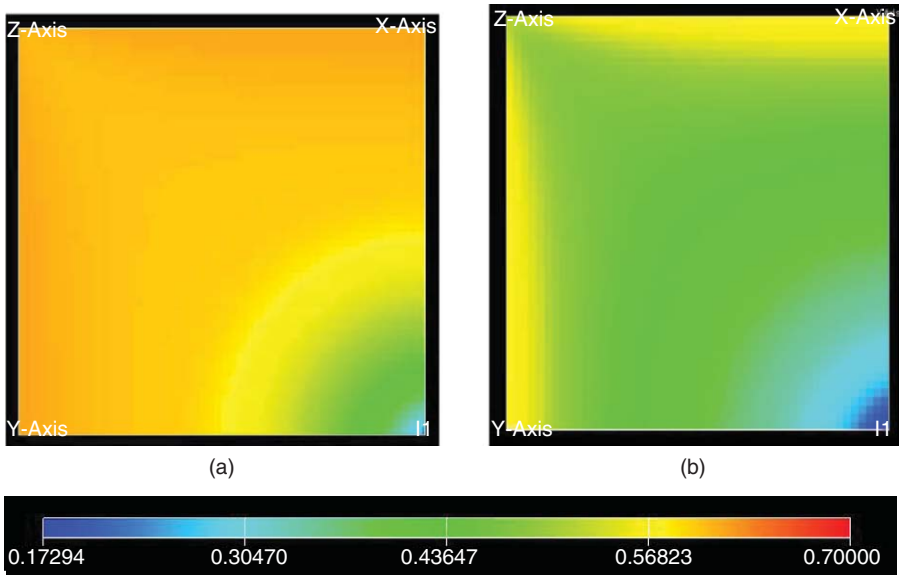

Fig. 8—Improved areal sweep in five-spot pattern during fines-assisted waterflooding after the breakthrough: (a) sweep for normal waterflooding; (b) areal saturation distribution over the flow pattern during fines-assisted waterflooding.

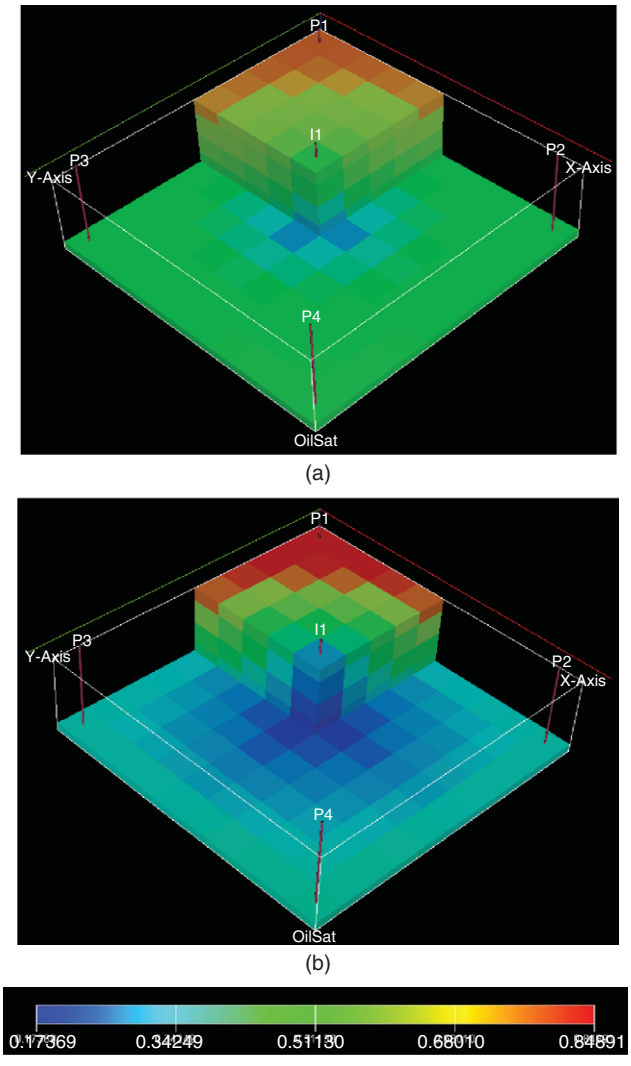

Fig. 9—Schema of well placing and oil saturation during waterflooding of five-layer cake reservoir after 0.4 PVI: (a) normal waterflooding; (b) fines-assisted waterflooding.

waterflooding in a monolayer five-spot pattern with areal heterogeneity SPE-9 was calculated (see blue continuous production curve in **Fig. 10**). Then, permeabilities and thicknesses of five layers have been selected to match the recovery-factor curve for

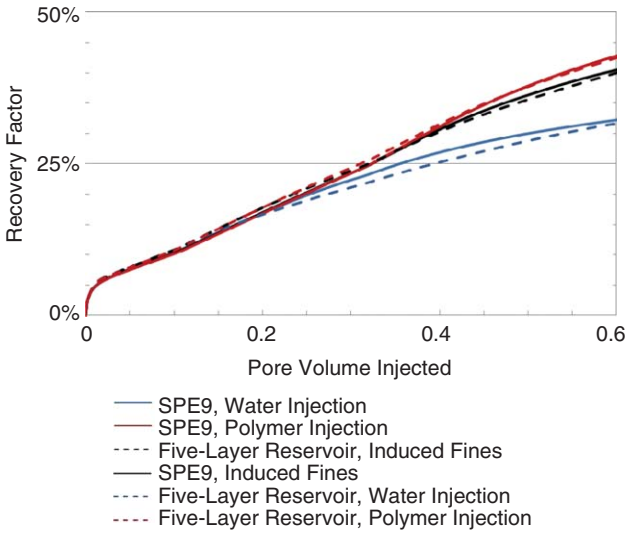

Fig. 10—Recovery factor.

TABLE 1—PERMEABILITY DISTRIBUTION IN FIVE-LAYER CAKE RESERVOIR

Layer	1	2	3	4	5
Permeability (md)	5	10	20	30	150
Thickness (ft)	49	90	79	39	29

the five-spot pattern with areal heterogeneity SPE-9; the corresponding parameters are given in Table 1. The recovery factors for normal waterflooding are 32% for both reservoirs (**Table 2**). The difference between the blue continuous and dashed production curves in Fig. 10 does not exceed 1.5%; the recovery factors are equal at the moment $t_D = 0.6$ PVI.

Inducing the formation damage by fines mobilization results in an increase of the injection pressure under the constant injection rate for both polymer injection and fines-assisted flooding. Usually, the rate program with decreasing $q(t)$ is designed for each reservoir case to keep the injection pressure below the fracturing pressure. Here, the rate program as well as the program for polymer concentration was taken from a polymer injection pilot test implemented in the Daqing oil field in China (Wang et al. 2008). The same rate program is used for the reservoir simulation of normal and fines-assisted waterfloodings.

Stepwise-decreasing polymer concentration and increasing injection rate were used in the Daqing pilot test. The polymer slug injection is carried out in four phases:

1. Polymer slug with concentration of 1,000 ppm was injected for 4.5 years at the constant rate of 245 stb/d.
2. Polymer slug with concentration of 700 ppm was injected for 9.3 years at the constant rate of 315 stb/d.
3. Polymer slug with concentration of 400 ppm was injected for 9 years at the constant rate of 420 stb/d.
4. This is followed up by water drive injection for the next 20 years.

In the programmed polymer slug, viscosity decreases from 40 cp on the slug front to 1 cp in the water drive. The polymer viscosity multiplier function $\mu_w\,(c_p)/\mu_w\,(0)$ is set to vary from unity at $C_p = 0$ to forty at $C_p = 1{,}000$ ppm [see Schlumberger Information Solutions (SIS) 2010]. Fluid properties are also taken from the Daqing test: oil viscosity $\mu_o = 9$ cp, initial reservoir pressure p_{res}=3000 psi, initial water saturation $s_{wi} = 0.15$, and maximum adsorption of HPAM polymer = 0.043 ppm. The polymer does not desorb in the water drive. The residual resistivity factor (RRF) is assumed to be 1.1.

Freshwater is also injected in a slug mode. A sensitivity study was conducted with respect to slug size. Increase of slug size results in the recovery factor increase, which gradually tends to that of the continuous freshwater injection. Yet the bottomhole injection pressure and the pressure drop across the reservoir gradually increase with increasing slug size. Therefore, there is a slug size with a recovery factor almost the same as that of the continuous freshwater injection, but with the significantly lower injection bottomhole pressure. These sizes have been found to be 0.04 PVI

TABLE 2—RECOVERY FACTOR AFTER 0.6 PVI

	Reservoir Model SPE-9	5-Layer Reservoir
Waterflood	32%	32%
Low-salinity waterflood with fines migration	40%	40%
Polymer flooding	43%	43%
Incremental recovery by low-salinity waterflood relative to normal waterflood $\Delta RF/RF_{WF}$	0.25	0.25

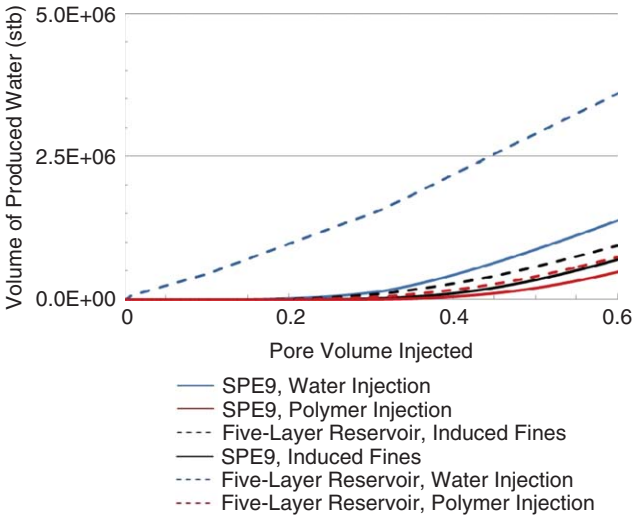

Fig. 11—Volume of produced water vs. time.

for the layer-cake reservoir and 0.06 PVI for the reservoir with SPE-9 heterogeneity.

The parameters of fines release and straining are taken from the experimental data by Lever and Dawe (1984) (Fig. 5) (i.e., it is assumed that these two reservoirs have the same properties as the core, used in the previously mentioned test). The RRF = 14. The polymer viscosity multiplier function $\mu_w\,(c_p)/\mu_w\,(0)$ is set to be unity in order to model freshwater injection.

Fig. 10 shows the incremental recovery for waterflood with fines and for polymer flooding compared with normal waterflooding. The recovery factors in five-layer-cake and SPE-9 reservoirs almost coincide, and the coincidence is exact at the moment of 0.6 PVI. The recovery with fines-assisted waterflooding (40%) at the moment 0.6 PVI is significantly higher than that for normal waterflooding (32%) and slightly lower than for polymer flooding (43%) (see Table 2). Therefore, fines-assisted waterflooding and polymer flooding both result in significant sweep-efficiency improvement if compared with that of the normal waterflood.

The induced formation damage caused by fines particle straining causes a significant decrease in production rates of water **(Fig. 11).** The reduction in the accumulated volume of produced water during low salinity flooding is significantly lower than during normal waterflooding and not noticeably higher if compared with polymer flooding: the amount of produced water at the moment $t_D = 0.6$ PVI in layer-cake reservoir for fines-assisted waterflooding is 3.7 times lower than with the normal waterflooding; for polymer injection it is 4.6 times lower than with the normal waterflooding. If compared with normal waterflooding in the reservoir with heterogeneity SPE-9, application of fines-assisted waterflooding results in reduction of produced water twice; application of polymer flood reduces the amount of produced water 2.8 times.

TABLE 3—FIELD WATER CUT AFTER 0.6 PV OF INJECTION

	Reservoir Model SPE-9	5-Layer Reservoir
Waterflood	0.78	0.75
Waterflood with fines migration	0.6	0.58
Polymer flooding	0.53	0.56

The same relationship holds for water cut in production wells. Fines-assisted waterflooding significantly decreases water cut if compared with normal waterflooding **(Table 3).** Polymer injection brings further reduction in water cut if compared with low-salinity flood **(Fig. 12).** Fig. 12 also shows the relationship between breakthrough times. The breakthrough time for fines-assisted waterflooding is significantly higher than that for normal waterflooding and lower than that for the polymer injection.

Higher bottomhole injection pressures are required for fines-assisted waterflooding (because of the induced permeability decline) and for polymer flooding (because of high viscosity of the polymer solution). For the case under investigation, the bottomhole pressure increase for polymer injection is higher than that for low-salinity flooding as depicted in **Fig. 13.**

Conclusion

The present work considers the simplified mechanism of oil recovery by low-salinity waterflooding; the model derived describes the decrease of relative permeability to water caused by release of fines by advancing low-salinity water caused in turn by expanding of the double electric layer and weakening the electrostatic force attaching fines to the rock surface. As was shown by Muecke (1979) and Sarkar and Sharma (1990), the damaging fines are mobile only in the water phase (Fig. 2). The equilibrium of fines is described by the torque balance of forces exerted upon the particles immersed in water phase. These effects explain the reduction in relative permeability for water and the consequent incremental recovery during low-salinity waterflooding observed by Hussein et al. (2012).

Compared with the previously derived fines-migration model in a one-phase environment with mobilization caused by flow-velocity increase, the model with fines lifting caused by the change in water salinity contains an extra equation for salt mass

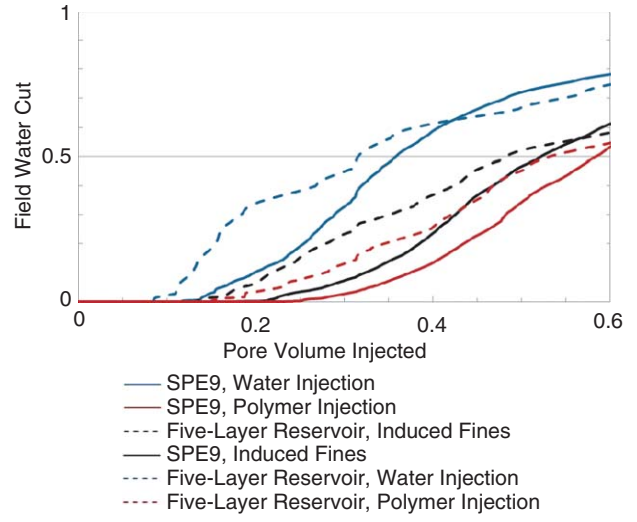

Fig. 12—Field water cut.

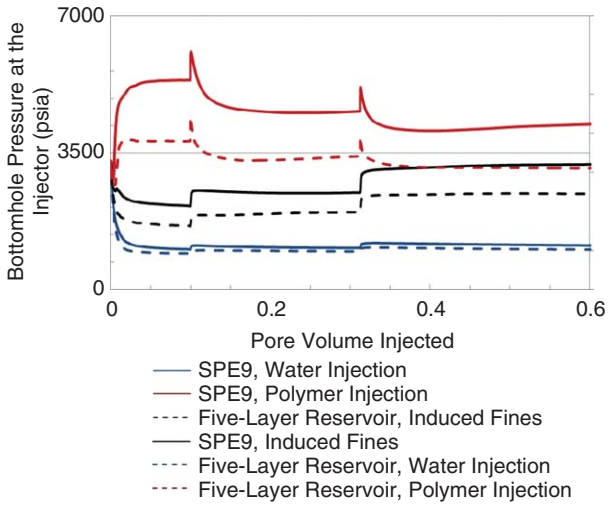

Fig. 13—Injector bottomhole pressure.

conservation. The alterations in the particle mechanical equilibrium by changes of both fluid velocity and salinity are captured by the erosion number, which depends on both factors. The maximum retention concentration for two-phase flow becomes a function of not only erosion number but also of saturation. It is assumed that the permeability reduction factor caused by particle capture is applied only to the permeability for the water phase. The governing system for two-phase flow with fines mobilization, migration, and capture contains seven equations.

The modified particle-detachment model with the maximum retained particle concentration as a function of water salinity was validated for single-phase flow of water through its comparison with laboratory-test data from the literature. The laboratory validation of this hypothesis for two-phase flow of immiscible water and oil is still required.

The large-scale approximation of the governing system of equations corresponds to an instant capture of mobilized particles. It reduces the number of equations in the governing system to four.

The large-scale equations for fines-assisted waterflooding can be solved numerically and used in open-source code reservoir simulators.

The large-scale model for two-phase flow with fines becomes equivalent to the two-phase immiscible-flow model for polymer flooding. The equivalence is established by the introduction of vanishing salt adsorption and resistivity factor for water phase, caused by adsorption. Therefore, the effects of fines release and capture because of changes in the composition of injected water can be included in the black-oil model for polymer flooding. Although only one example of the decreasing of salinity of the injected water was considered, a similar modeling process could be followed for the alteration of any property of the injected water that results in the release of fines, such as pH, concentrations of different ions, and temperature. The equivalence of the models allows using the commercial simulators with a polymer-flooding option for modeling the fines-assisted waterflood.

The restriction of independence of the polymer adsorption of saturation, which is typical for the commercial reservoir simulators, corresponds to independence of the maximum retention function of saturation. Because the salinity front lags behind the saturation front, the fines detachment occurs in the reservoir areas where oil saturation is close to the residual saturation, allowing the fixing of the constant residual oil saturation in the maximum retention function.

The discussed effects of fines-assisted waterflooding can be sound in the reservoirs with significant fines content in the rock that can be released by injected low-salinity water. In this case, the main improved recovery mechanism would be the permeability reduction in swept areas by the mobilized and strained fines and the consequent diversion of the injected water into unswept zones. This results in a prolongation of the "dry" water-free production period, reduced water cut during the initial after-the-breakthrough period, and reduced residual reserves.

For the modeled field case, the recovery factor after 0.6 PVI increases from 32% for normal waterflooding to 40% at the fines-assisted waterflooding, and up to 43% at programmed polymer slug injection. If compared with normal waterflooding, application of fines-assisted flooding results in a 2- to 3.7-times decrease in produced water; application of polymer flooding decreases the amount of produced water 2.8 to 4.6 times. Fines-assisted flooding results in significant reduction of water cut and increase of the breakthrough time if compared with the normal waterflood; the water-cut reduction and waterless production period increase with polymer flooding are higher: water cut decreases from 0.77 to 0.59 because of fines-assisted flooding being 0.55 for polymer flooding after 0.6 PVI. Yet the induced fines migration results in increase of the pressure drop across the reservoir or in the injection-rate decrease because of decrease of permeability in the swept zone.

Whether fines migration is the most relevant mechanism in low-salinity waterflooding is debatable because, apart from supporting evidence, there are plenty of contradicting observations. Detailed laboratory studies must be performed to resolve this doubt in every specific situation of mineral composition of rock, water, and oil chemistry.

Nomenclature

A = area, L^2, m^2
A_{132} = Hamaker constant, MLT^{-2}, J
c = concentration of suspended particles
c_a = polymer adsorption concentration
c_p = polymer concentrations in the aqueous phase
c_p^0 = polymer concentrations in the injected water
C = normalized concentration of suspended particles
f = fractional flow of water
F_d = drag force, MLT^{-2}, N
F_e = electrostatic force, MLT^{-2}, N
F_g = gravitational force, MLT^{-2}, N
F_l = lifting force, MLT^{-2}, N
h_c = cake thickness, L, m
H = reservoir thickness, L, m
k = absolute permeability, L^2, mD
k_B = Boltzmanńs constant, $MLT^{-2}\theta^{-1}$, J/K,
k_o = initial absolute permeability, L^2, mD
k_{ro} = oil relative permeability
k_{rw} = water relative permeability
l_d = lever for drag force, L, m
l_n = lever for normal force, L, m
L = reservoir length, L, m
M = ratio between viscosities of water and oil
n = pores density in a cross section, L^{-2}, m^{-2}
p = pressure, $ML^{-1}T^{-2}$, Pa
P = dimensionless pressure
q = volumetric flow rate, L^3T^{-1}, m^3/s
r_p = particle radius, L, m
r_s = pore radius, L, m
R_k = resistance factor
s = water saturation
S_a = dimensionless concentration of attached particles
S_s = dimensionless concentration of strained particles
t = time, T, s
t_D = dimensionless time
T = temperature, K, θ
u = dimensionless velocity of the overall two-phase flux
u_p = averaged velocity in a single capillary, LT^{-1}, m/s
U = overall flow velocity, LT^{-1}, m/s
V = potential, MLT^{-2}, J
V_{BR} = Born potential, MLT^{-2}, J
V_{DLR} = double electric layer potential, MLT^{-2}, J
V_{LVA} = London-van-der-Waals potential, MLT^{-2}, J
W = reservoir width, L, m
x = linear co-ordinate, L, m
x_D = dimensionless length
y = dimensionless velocity
β = formation damage coefficient
γ = brine ionic strength, $molL^{-3}$, mol/lit
γ_i = reservoir initial brine ionic strength, $molL^{-3}$, mol/lit
γ^0 = ionic strength of the injected brine, $molL^{-3}$, mol/lit
ε = torque ratio(erosion number)
κ = inverse Debye length, m, L
λ_s = filtration coefficient for straining, L^{-1}, 1/m
μ_o = oil dynamic viscosity, $ML^{-1}T^{-1}$, cp
μ_w = water dynamic viscosity, $ML^{-1}T^{-1}$, cp
ρ_o = oil density, ML^{-3}, kg/m^3
ρ_w = water density, ML^{-3}, kg/m^3
σ = volumetric concentration of captured particles
σ_a = volumetric concentration of attached particles
σ_{ao} = initial volumetric concentration of attached particles
σ_{cr} = maximum volumetric concentration of captured particles
σ_s = volumetric concentration of strained particles
ϕ = porosity
ϕ_c = cake porosity
χ = lifting coefficient
ψ_{01} = surface potential of particle, mV, MLT^{-2}

ψ_{02} = surface potential of collector, mV, MLT^{-2}
ω = dimensionless drag constant

Acknowledgments

The authors thank P. Lemon, T. Rodrigues, I. Abbasy, and K. Boyle (Santos Ltd, Australia); and F. Machado, A.L. and S. de Souza (Petrobras, Brazil) for detailed discussions of the field applications, for support, and for encouragement. Bedrikovetsky is grateful to P. Currie (Delft University of Technology), A. Shapiro (Technical University of Denmark) and M. Haghighi (University of Adelaide) for long-time cooperation in formation damage. Special thanks are given to A. Badalyan and Z. You for editing the text. Detailed discussions with colleagues from Shell Research/Delft University—H. Bruining, C. van Kruijdjik, R. Farajzadeh, and H Mahani—are greatly acknowledged.

The work is sponsored by Santos Ltd. and a Discovery Grant of the Australian Research Council.

References

Akhatov, I.S., Hoey, J.M., Swenson, O.F. et al. 2008. Aerosol focusing in micro-capillaries: Theory and experiment. *J. Aerosol Sci.* **39** (8): 691–709. http://dx.doi.org/10.1016/j.jaerosci.2008.04.004.

Altmann, J. and Ripperger, S. 1997. Particle deposition and layer formation at the crossflow microfiltration. *J. Membr. Sci.* **124** (1): 119–128. http://dx.doi.org/10.1016/s0376-7388(96)00235-9.

Bedrikovetsky, P., Marchesin, D., Shecaira, F. et al. 2001. Characterization of deep bed filtration system from laboratory pressure drop measurements. *J. Pet. Sci. Eng.* **64** (3): 167–177. http://dx.doi.org/10.1016/S0920-4105(01)00159-0.

Bedrikovetsky, P. 2008. Upscaling of Stochastic Micro Model for Suspension Transport in Porous Media. *Transport Porous Media* **75** (3): 335–369. http://dx.doi.org/10.1007/s11242-008-9228-6.

Bedrikovetsky, P., Siqueira, F., Furtado, C. et al. 2011. Modified Particle Detachment Model for Colloidal Transport in Porous Media. *Transport Porous Media* **86** (2): 353–383. http://dx.doi.org/10.1007/s11242-010-9626-4.

Bedrikovetsky, P., Zeinijahromi, A., Siqueira, F. et al. 2012. Particle Detachment Under Velocity Alternation During Suspension Transport in Porous Media. *Transport Porous Media* **91** (1): 173–197. http://dx.doi.org/10.1007/s11242-011-9839-1.

Bennion, D.B. and Thomas, F.B., 2005. Formation Damage Issues Impacting the Productivity of Low Permeability, Low Initial Water Saturation Gas Producing Formations. *Journal of Energy Resources Technology* **127** (3): 240–247.

Berg, S., Cense, A.W., Jansen, E. et al. 2010. Direct Experimental Evidence of Wettability Modification By Low Salinity. *Petrophysics* **51** (5): 314–322. SPWLA-2010-v51n5a3.

Bergendahl, J. and Grasso, D. 2000. Prediction of colloid detachment in a model porous media: hydrodynamics. *Chem. Eng. Sci.* **55** (9): 1523–1532. http://dx.doi.org/10.1016/s0009-2509(99)00422-4.

Bernard, G. 1967. Effect of Floodwater Salinity on Recovery Of Oil from Cores Containing Clays. Presented at the SPE California Regional Meeting, Los Angeles, California, USA, 26–27 October. SPE-1725-MS. http://dx.doi.org/10.2118/1725-MS.

Bradford, S.A., Torkzaban, S., and Simunek, J. 2011a. Modeling colloid transport and retention in saturated porous media under unfavorable attachment conditions. *Water Resour. Res.* **47** (10): W10503. http://dx.doi.org/10.1029/2011wr010812.

Bradford, S.A., Torkzaban, S., and Wiegmann, A. 2011b. Pore-scale Simulations To Determine The Applied Hydrodynamic Torque And Colloid Immobilization. *Vadose Zone J.* **10** (1): 252–261. http://dx.doi.org/10.2136/vzj2010.0064.

Cense, A., Berg, S., Bakker, K. et al. 2011. Direct Visualization of Designer Water Flooding in Model Experiments. Presented at the SPE Enhanced Oil Recovery Conference, Kuala Lumpur, 19–21 July. SPE-144936-MS. http://dx.doi.org/10.2118/144936-MS.

Chauveteau, G., Nabzar, L., and Coste, J.-P. 1998. Physics and Modeling of Permeability Damage Induced by Particle Deposition. Presented at the SPE Formation Damage Control Conference, Lafayette, Louisiana, USA, 18–19 February. SPE-39463-MS. http://dx.doi.org/10.2118/39463-MS.

Civan, F. 2007. *Reservoir Formation Damage: Fundamentals, Modeling, Assessment, and Mitigation*, second edition. Burlington, Massachusetts: Gulf Professional Publishing/Elsevier.

Civan, F. 2010. Non-isothermal Permeability Impairment by Fines Migration and Deposition in Porous Media including Dispersive Transport. *Transport Porous Media* **85** (1): 233–258. http://dx.doi.org/10.1007/s11242-010-9557-0.

Derjaguin, B.V. and Landau, L. 1941. Theory of the Stability of Strongly Charged Lyophobic Sols and of the Adhesion of Strongly Charged Particles in Solutions of Electrolytes. *Acta Phys. Chim. URSS* **14** (1941): 633–662. http://dx.doi.org/citeulike-article-id:2925659.

Elimelech, M., Jia, X., Gregory, J. et al. 1995. *Particle Deposition and Aggregation: Measurement, Modelling and Simulation*, hardcover edition. Woburn, Massachusetts: Colloid and Surface Engineering Series, Butterworth-Heinemann.

Freitas, A.M. and Sharma, M.M. 2001. Detachment of Particles from Surfaces: An AFM Study. *J. Colloid Interface Sci.* **233** (1): 73–82. http://dx.doi.org/10.1006/jcis.2000.7218.

Fogden, A., Kumar, M., Morrow, N.R. et al. 2011. Mobilization of Fine Particles during Flooding of Sandstones and Possible Relations to Enhanced Oil Recovery. *Energy Fuels* **25** (4): 1605–1616. http://dx.doi.org/10.1021/ef101572n.

Gregory, J. 1981. Approximate expressions for retarded van der waals interaction. *J. Colloid Interface Sci.* **83** (1): 138–145. http://dx.doi.org/10.1016/0021-9797(81)90018-7.

Hunter, R.J. 2001. *Foundations of Colloid Science*. Oxford, UK: Oxford University Press.

Hussein, F., Zeinijahromi, A., Bedrikovetsky, P. et al. 2012. Improved Oil Recovery with Waterflooding by Mobilising Fines (laboratory-based incremental recovery). Presented at the North Africa Technical Conference and Exhibition, Cairo, Egypt, 20–22 February. SPE-149704-PP.

Israelachvili, J.N. 2006. *Intermolecular and Surface Forces*, second edition. London: Academic Press.

Jerauld, G.R., Lin, C.Y., Webb, K.J. et al. 2008. Modeling Low-Salinity Waterflooding. *SPE Res Eval & Eng* **11** (6): 1000–1012. SPE-102239-PA. http://dx.doi.org/10.2118/102239-PA.

Ju, B., Fan, T., Wang, X. et al. 2007. A new simulation framework for predicting the onset and effects of fines mobilization. *Transport Porous Media* **68** (2): 265–283. http://dx.doi.org/10.1007/s11242-006-9044-9.

Ju, B. and Fan, T. 2009. Experimental study and mathematical model of nanoparticle transport in porous media. *Powder Technol.* **192** (2): 195–202. http://dx.doi.org/10.1016/j.powtec.2008.12.017.

Kang, S.-T., Subramani, A., Hoek, E.M.V. et al. 2004. Direct observation of biofouling in cross-flow microfiltration: mechanisms of deposition and release. *J. Membr. Sci.* **244** (1–2): 151–165. http://dx.doi.org/10.1016/j.memsci.2004.07.011.

Khilar, K.C. and Fogler, H.S. 1998. *Migration of Fines in Porous Media*. Dordrecht, The Netherlands: Theory and Applications of Transport in Porous Media, Kluwer Academic Publishers.

Khilar, K.C., Fogler, H.S., and Ahluwalia, J.S. 1983. Sandstone water sensitivity: Existence of a critical rate of salinity decrease for particle capture. *Chem. Eng. Sci.* **38** (5): 789–800. http://dx.doi.org/10.1016/0009-2509(83)80188-2.

Lager, A., Webb, K.J., Black, C.J.J. et al. 2008. Low-Salinity Oil Recovery—An Experimental Investigation. *Petrophysics* **49** (1): 28–35. http://dx.doi.org/2008-v49n1a2.

Lake, L.W. 1989. *Enhanced Oil Recovery*. Englewood Cliffs, New Jersey: Prentice Hall.

Landau, L.D. and Lifshitz, E.M. 1980. *Statistical Physics, Part* **1**, third edition, trans. J.B. Sykes and M.J. Kearsley, Vol. 5. Oxford, UK: Course in Theoretical Physics, Butterworth-Heinemann.

Lemon, P., Zeinijahromi, A., Bedrikovetsky, P. et al. 2011. Effects of Injected-Water Salinity on Waterflood Sweep Efficiency Through Induced Fines Migration. *J Can Pet Technol* **50** (9): 82–94. SPE-140141-PA. http://dx.doi.org/10.2118/140141-PA.

Lever, A. and Dawe, R.A. 1984. Water-Sensitivity and Migration of Fines in the Hopeman Sandstone. *J. Pet. Geol* **7** (1): 97–107. http://dx.doi.org/10.1111/j.1747-5457.1984.tb00165.x.

Li, X., Lin, C.-L., Miller, J.D. et al. 2006. Role of Grain-to-Grain Contacts on Profiles of Retained Colloids in Porous Media in the Presence of an

Energy Barrier to Deposition. *Environ. Sci. Technol.* **40** (12): 3769–3774. http://dx.doi.org/10.1021/es052501w.

Liu, X. and Civan, F. 1996. Formation Damage and Filter Cake Buildup in Laboratory Core Tests: Modeling and Model-Assisted Analysis. *SPE Form Eval* **11** (1): 26–30. SPE-25215-PA. http://dx.doi.org/10.2118/25215-PA.

Ligthelm, D.J., Gronsveld, J., Hofman, J. et al. 2009. Novel Waterflooding Strategy by Manipulation of Injection Brine Composition. Presented at the EUROPEC/EAGE Conference and Exhibition, Amsterdam, 8–11 June. SPE-119835-MS. http://dx.doi.org/10.2118/119835-MS.

Mahani, H., Sorop, T., Ligthelm, D.J. et al. 2011. Analysis of Field Responses to Low-salinity Waterflooding in Secondary and Tertiary Mode in Syria. Presented at the SPE EUROPEC/EAGE Annual Conference and Exhibition, Vienna, Austria, 23–26 May. SPE-142960-MS. http://dx.doi.org/10.2118/142960-MS.

Miranda, R.M. and Underdown, D.R. 1993. Laboratory Measurement of Critical Rate: A Novel Approach for Quantifying Fines Migration Problems. Presented at the SPE Production Operations Symposium, Oklahoma City, Oklahoma, USA, 21–23 March. SPE-25432-PA. http://dx.doi.org/10.2118/25432-MS.

Mojarad, R.S. and Settari, A. 2007. Coupled Numerical Modelling of Reservoir Flow with Formation Plugging. *J Can Pet Technol* **46** (3): 54–59. JCPT Paper No. 07-03-05. http://dx.doi.org/10.2118/07-03-05.

Morrow, N. and Buckley, J. 2011. Improved Oil Recovery by Low-Salinity Waterflooding. *SPE Journal of Petroleum Technology* **63** (5): 106–112. SPE-129421-MS. http://dx.doi.org/10.2118/129421-MS.

Muecke, T.W. 1979. Formation Fines and Factors Controlling Their Movement in Porous Media. *J Pet Technol* **31** (2): 144–150. SPE-7007-PA. http://dx.doi.org/10.2118/7007-PA.

Mungan, N. 1965. Permeability Reduction Through Changes in pH and Salinity. *J Pet Technol* **17** (12): 1449–1453. SPE-1283-PA. http://dx.doi.org/10.2118/1283-PA.

Nabzar, L., Chauveteau, G., and Roque, C. 1996. A New Model for Formation Damage by Particle Retention. Presented at the SPE Formation Damage Control Conference, Lafayette, Louisiana, USA, 14–15 February. SPE-31119-MS. http://dx.doi.org/10.2118/31119-MS.

O'Neill, M.E. 1968. A sphere in contact with a plane wall in a slow linear shear flow. *Chem. Eng. Sci.* **23** (11): 1293–1298. http://dx.doi.org/10.1016/0009-2509(68)89039-6.

Ochi, J. and Vernoux, J.-F. 1998. Permeability decrease in sandstone reservoirs by fluid injection: Hydrodynamic and chemical effects. *J. Hydrol.* **208** (3–4): 237–248. http://dx.doi.org/10.1016/s0022-1694(98)00169-3.

Pang, S. and Sharma, M.M. 1997. A Model for Predicting Injectivity Decline in Water-Injection Wells. *SPE Form Eval* **12** (3): 194–201. SPE-28489-PA. http://dx.doi.org/10.2118/28489-PA.

Payatakes, A.C., Tien, C., and Turian, R.M. 1973. A new model for granular porous media: Part I. Model formulation. *AIChE J.* **19** (1): 58–76. http://dx.doi.org/10.1002/aic.690190110.

Payatakes, A.C., Rajagopalan, R., and Tien, C. 1974. Application of porous medium models to the study of deep bed filtration. *The Canadian Journal of Chemical Engineering* **52** (6): 727–731. http://dx.doi.org/10.1002/cjce.5450520605.

Pu, H., Xie, X., Yin, P. et al. 2010. Low Salinity Waterflooding and Mineral Dissolution. Presented at the SPE Annual Technical Conference and Exhibition, Florence, Italy, 19–22 September. SPE-134042-MS. http://dx.doi.org/10.2118/134042-MS.

Rivet, S.M., Lake, L.W., and Pope, G.A. 2010. A Coreflood Investigation of Low-Salinity Enhanced Oil Recovery. Presented at the SPE Annual Technical Conference and Exhibition, Florence, Italy, 19–22 September. SPE-134297-MS. http://dx.doi.org/10.2118/134297-MS.

Rousseau, D., Hadi, L., and Nabzar, L. 2008. Injectivity Decline From Produced-Water Reinjection: New Insights on In-Depth Particle-Deposition Mechanisms. *SPE Prod & Oper* **23** (4): 525–531. SPE-107666-PA. http://dx.doi.org/10.2118/107666-PA.

Saffman, P.G. 1965. The lift on a small sphere in a slow shear flow. *J. Fluid Mech.* **22** (02): 385–400. http://dx.doi.org/doi:10.1017/S0022112065000824.

Saffmann, P.G. 1968. The lift on a small sphere in a slow shear flow - Corrigendum. *J. Fluid Mech.* **31** (03): 624. http://dx.doi.org/10.1017/S0022112068999990.

Sarkar, A.K. and Sharma, M.M. 1990. Fines Migration in Two-Phase Flow. *J Pet Technol* **42** (5): 646–652. SPE-17437-PA. http://dx.doi.org/10.2118/17437-PA.

Sbai, M.A. and Azaroual, M. 2011. Numerical modeling of formation damage by two-phase particulate transport processes during CO2 injection in deep heterogeneous porous media. *Adv. Water Resour.* **34** (1): 62–82. http://dx.doi.org/10.1016/j.advwatres.2010.09.009.

Schembre, J.M. and Kovscek, A.R. 2005. Mechanism of Formation Damage at Elevated Temperature. *J. Energy Resour. Technol.* **127** (3): 171–180. http://dx.doi.org/10.1115/1.1924398.

Scheuerman, R.F. and Bergersen, B.M. 1990. Injection-Water Salinity, Formation Pretreatment, and Well-Operations Fluid-Selection Guidelines. *J Pet Technol* **42** (7): 836–845. SPE-18461-PA. http://dx.doi.org/10.2118/18461-PA.

Schlumberger Information Solutions (SIS). 2010. ECLIPSE Reservoir Engineering Software, http://www.slb.com/services/software/reseng.aspx.

Sharma, M.M. and Yortsos, Y.C. 1987a. Transport of particulate suspensions in porous media: Model formulation. *AIChE J.* **33** (10): 1636–1643. http://dx.doi.org/10.1002/aic.690331007.

Sharma, M.M. and Yortsos, Y.C. 1987b. A network model for deep bed filtration processes. *AIChE J.* **33** (10): 1644–1653. http://dx.doi.org/10.1002/aic.690331008.

Sharma, M.M. and Yortsos, Y.C. 1987c. Fines migration in porous media. *AIChE J.* **33** (10): 1654–1662. http://dx.doi.org/10.1002/aic.690331009.

Takahashi, S. and Kovscek, A.R. 2010. Wettability estimation of low-permeability, siliceous shale using surface forces. *J. Pet. Sci. Eng.* **75** (1–2): 33–43. http://dx.doi.org/10.1016/j.petrol.2010.10.008.

Tang, G.-Q. and Morrow, N.R. 1999. Influence of brine composition and fines migration on crude oil/brine/rock interactions and oil recovery. *J. Pet. Sci. Eng.* **24** (2–4): 99–111. http://dx.doi.org/10.1016/S0920-4105(99)00034-0.

Tufenkji, N. and Elimelech, M. 2003. Correlation Equation for Predicting Single-Collector Efficiency in Physicochemical Filtration in Saturated Porous Media. *Environ. Sci. Technol.* **38** (2): 529–536. http://dx.doi.org/10.1021/es034049r.

Tufenkji, N. 2007. Colloid and Microbe Migration in Granular Environments: A Discussion of Modelling Methods. In *Colloidal Transport in Porous Media*, F.H. Frimmel, F. von der Kammer, and H.-C. Flemming, Chap. 5, 119–142. Berlin, Germany: Springer-Verlag.

Valdya, R.N. and Fogler, H.S. 1992. Fines Migration and Formation Damage: Influence of pH and Ion Exhange. *SPE Prod Eng* **7** (4): 325–330. SPE-19413-PA. http://dx.doi.org/10.2118/19413-PA.

Wang, D.M., Seright, R.S., Shao, Z. et al. 2008. Key Aspects of Project Design for Polymer Flooding at the Daqing Oil Field. *SPE Res Eval & Eng* **11** (6): 1117–1124. SPE-109682-PA. http://dx.doi.org/10.2118/109682-PA.

Yildiz, H.O. and Morrow, N.R. 1996. Effect of brine composition on recovery of Moutray crude oil by waterflooding. *J. Pet. Sci. Eng.* **14** (3–4): 159–168. http://dx.doi.org/10.1016/0920-4105(95)00041-0.

Yuan, H. and Shapiro, A.A. 2010. A mathematical model for non-monotonic deposition profiles in deep bed filtration systems. *Chem. Eng. J. (Lausanne)* **166** (1): 105–115. http://dx.doi.org/10.1016/j.cej.2010.10.036.

Yuan, H. and Shapiro, A.A. 2011. Induced migration of fines during waterflooding in communicating layer-cake reservoirs. *J. Pet. Sci. Eng.* **78** (3–4): 618–626. http://dx.doi.org/10.1016/j.petrol.2011.08.003.

Zeinijahromi, A., Lemon, P., and Bedrikovetsky, P. 2011a. Effects of induced fines migration on water cut during waterflooding. *J. Pet. Sci. Eng.* **78** (3–4): 609–617. http://dx.doi.org/10.1016/j.petrol.2011.08.005.

Zeinijahromi, A., Nguyen, P.T., and Bedrikovetsky, P.G. 2011b. Taking Advantage of Fines-Migration-Induced Formation Damage for Improved Waterflooding (Reservoir Simulation using Polymer Flood Option). Presented at the SPE European Formation Damage Conference, Noordwijk, The Netherlands, 7–10 June. SPE-144009-MS. http://dx.doi.org/10.2118/144009-MS.

Zhang, Y. and Morrow, N.R. 2006. Comparison of Secondary and Tertiary Recovery With Change in Injection Brine Composition for Crude Oil/Sandstone Combinations. Presented at the SPE/DOE Symposium on Improved Oil Recovery, Tulsa, 22–26 April. SPE-99757-MS. http://dx.doi.org/10.2118/99757-MS.

Appendix A—Calculation of the Maximum Retention Function

Let us calculate the maximum retention function for a bundle of parallel capillary distributed by radius with density distribution function $f(r_p)$. Fig. 1b shows the forces exerting a single fine particle on the surface of an internal filter cake or of a pore. The drag force is given by the expression (O'Neill 1968; Altmann and Ripperger 1997; Bergendahl and Grasso 2000) derived from the analytical solution of the Navier-Stokes equations for flow around a finite-size particle fixed on the plane

$$F_d = \frac{\omega\pi\mu r_s^2 u_p(r_p)}{r_p - h_c}, \quad \ldots\ldots\ldots\ldots\ldots\ldots\ldots\ldots\ldots\ldots (A\text{-}1)$$

where the dimensionless drag constant ω is an empirical coefficient varying in the range of 10–60.

The general form of the lifting force is given by

$$F_l = \chi r_s^3 \sqrt{\frac{\rho\mu u_p(r_p)^3}{(r_p - h_c)^3}} \quad \ldots\ldots\ldots\ldots\ldots\ldots\ldots\ldots\ldots\ldots (A\text{-}2)$$

where the lifting coefficient χ is given as 48.8 by Kang et. al. (2004), while Altmann and Ripperger (1997) gave a value of 1,190. A similar expression is used by Akhatov et al. (2008). The general form (Eq. A-2) was obtained using the derivations by Saffmann (1965, 1968).

More precise formulae (Eqs. A-2 and A-3) for particles with sizes comparable with the pore radii can be obtained by numerical solutions of Navier-Stokes equations using computational fluid dynamics software packages.

The expression for buoyancy force is

$$F_g = \frac{4\pi r_s^3}{3}\Delta\rho g. \quad \ldots\ldots\ldots\ldots\ldots\ldots\ldots\ldots\ldots\ldots (A\text{-}3)$$

The total electrostatic force is derivative of the potential energy

$$F_e = -\frac{\partial V}{\partial h}, \quad \ldots\ldots\ldots\ldots\ldots\ldots\ldots\ldots\ldots\ldots (A\text{-}4)$$

where the total energy is the sum of the London-van-der-Waals double electric layer and Born potentials, given by the so-called DLVO (Derjagin-Landau-Verwey-Overbeek) theory (Derjagin and Landau 1941; Gregory 1981; Elimelech et al. 1995; Khilar and Fogler 1998; Israelachvili 2006):

$$\begin{aligned}
V_{LVA} &= -\frac{A_{132}}{6}\left[\frac{2(1+Z)}{Z(2+Z)} + \ln\left(\frac{Z}{2+Z}\right)\right]; \quad Z = \frac{h}{r_s} \\
V_{DLR} &= \frac{\varepsilon_0 D_e r_s}{4}\left[\begin{array}{l} 2\psi_{01}\psi_{02}\ln\left(\dfrac{1+\exp(-\kappa h)}{1-\exp(-\kappa h)}\right) \\ \qquad -(\psi_{01}^2+\psi_{02}^2)\ln\left(1-\exp(-2\kappa h)\right)\end{array}\right] \\
V_{BR} &= \frac{A_{132}}{7560}\left(\frac{\sigma_{LJ}}{r_s}\right)^6\left[\frac{8+Z}{(2+Z)^7} + \frac{6-Z}{Z^7}\right] \\
V &= V_{LVA} + V_{DLR} + V_{BR}. \quad \ldots\ldots\ldots\ldots\ldots\ldots (A\text{-}5)
\end{aligned}$$

Here, A_{132} is the Hamaker constant; h is the surface-to-surface separation length; ε_0 is the electric constant (permittivity of free space); D_e is the dielectric constant; ψ_{01} and ψ_{02} are the surface potentials of particles and collectors-grains, respectively; r_s is the particle size; and σ_{LJ} is atomic collision diameter in Lennard-Jones potential (Landau and Lifshitz 1980). The inverse Debye length κ is

$$\kappa = \sqrt{\left(\frac{e^2\sum \nu_i z_i^2}{\varepsilon_0 D k_B T}\right)},$$

where k_B is the Boltzmanńs constant, ν_i is a bulk ith ion concentration as defined by the number of ions per unit volume, z_i is a valence of the ith ion, and e is the electron charge $e = 1.6\times10^{-19}$ C. For aqueous solutions under normal temperature, this formula simplifies as

$$\kappa = 0.73 * 10^8\sqrt{\sum C_{mi} z_i^2},$$

where C_{mi} is the molar ith ion concentration in moles/m^3 (Elimelech et al. 1995).

Following Frietas and Sharma (2001), we assume that

$$\frac{l_D}{l_n} = \sqrt{3}. \quad \ldots\ldots\ldots\ldots\ldots\ldots\ldots\ldots\ldots\ldots (A\text{-}6)$$

Substitution of the expressions for forces (Eqs. A-1 through A-3, Eq. A-6) into the torque balance (Eq. 1) yields

$$\begin{aligned}
1 + \frac{4\pi r_s^3}{3F_e}\Delta\rho g - \chi\frac{\sqrt{\rho F_e}}{\mu}\sqrt{\frac{\mu^3 r_s^6 u_p(r_p)^3}{r_p^3\left(1-h_c/r_p\right)^3 F_e^3}} \\
= \frac{\sqrt{3}\omega\pi\mu r_s^2 u_p(r_p)}{r_p\left(1-h_c/r_p\right)F_e}.
\end{aligned} \quad \ldots\ldots (A\text{-}7)$$

Introducing dimensionless velocity y in capillary

$$y = \frac{\mu r_s^2 u_p(r_p)}{r_p\left(1-h_c/r_p\right)F_e} \quad \ldots\ldots\ldots\ldots\ldots\ldots\ldots\ldots (A\text{-}8)$$

yields the cubic equation with respect to unknown $y^{1/2}$:

$$\begin{aligned}
&y^{3/2} + \frac{\sqrt{3}\omega\pi\mu}{\chi\sqrt{\rho F_e}}y - \frac{\left(1+\dfrac{4\pi r_s^3}{3F_e}\Delta\rho g\right)\mu}{\chi\sqrt{\rho F_e}} = 0, \\
&y = F\left(\frac{\sqrt{3}\omega\pi\mu}{\chi\sqrt{\rho F_e}}, \frac{\left(1+\dfrac{4\pi r_s^3}{3F_e}\Delta\rho g\right)\mu}{\chi\sqrt{\rho F_e}}\right)
\end{aligned} \quad \ldots\ldots\ldots (A\text{-}9)$$

so dimensionless velocity x is a function of two dimensionless parameters. The expression for cake thickness $h_c(r_p)$ follows from Eq. A-8:

$$h_c(r_p) = r_p - \frac{\mu r_s^2 u_p(r_p)}{F_e y}. \quad \ldots\ldots\ldots\ldots\ldots\ldots\ldots (A\text{-}10)$$

The overall velocity U in the parallel bundle of capillary follows from the Poiseuille formula

$$U = -\frac{\pi n}{8\mu}\int_0^\infty r_p^4 f(r_p)dr_p\nabla p \quad \ldots\ldots\ldots\ldots\ldots\ldots (A\text{-}11)$$

$$n = \frac{\phi}{\pi\int_0^\infty r_p^2 f(r_p)dr_p}, \quad \ldots\ldots\ldots\ldots\ldots\ldots\ldots\ldots (A\text{-}12)$$

where the capillary density in the cross section can be determined from porosity.

The averaged velocity in a single capillary,

$$u_p(r_p) = -\frac{\pi r_p^3}{8\mu}\nabla p, \quad \ldots\ldots\ldots\ldots\ldots\ldots\ldots\ldots (A\text{-}13)$$

can be expressed through the average velocity accounting for Eqs. A-11 and A-12 as

$$u_p(r_p) = \frac{\pi r_p^2\int_0^\infty r_p^2 f(r_p)dr_p}{\phi\int_0^\infty r_p^2 f(r_p)dr_p}U. \quad \ldots\ldots\ldots\ldots\ldots\ldots (A\text{-}14)$$

The concentration of attached particles is

$$\sigma_{cr}(U) = n\pi(1-\phi_c) \int_0^{\infty} \left[r_p^2 - \left(r_p - h_c(r_p)\right)^2\right] f(r_p) dr_p. \quad \ldots\ldots (A\text{-}15)$$

Substitution of Eqs. A-10 through A-14 into the expression for attached concentration in Eq. A-15 results in an explicit expression for the maximum retention function $\sigma_{cr}(U)$.

For a single tube, the torque ratio is a function of average cross-sectional velocity $u(r_p)$:

$$\varepsilon(r_p) = \frac{\sqrt{3}F_d + F_l}{F_e + F_g} = \frac{\dfrac{\sqrt{3}\omega\pi\mu r_s^2 u_p(r_p)}{r_p} + \chi r_s^3 \sqrt{\dfrac{\rho\mu u_p^3(r_p)}{r_p^3}}}{F_e + F_g}. \quad \ldots\ldots (A\text{-}16)$$

Substituting the expression for average velocity in each capillary (Eq. A-14) into Eq. A-16, and calculating the averaged value for the torque ratio,

$$\bar{\varepsilon}(U) = \int_0^{\infty} \varepsilon(r_p) f(r_p) dr_p \quad \ldots\ldots\ldots\ldots\ldots\ldots (A\text{-}17)$$

results in the same functional dependency of σ_{cr} on average velocity U as in Eq. A-16. Therefore, the σ_{cr} dependency of averaged torque ratio follows from Eq. A-17.

Appendix B—Dimensionless Equations for Waterflood With Fines Migration

Introducing dimensionless coordinates, time, and concentrations into a system of basic equations for two-phase immiscible flow with fines migration (Eqs. 7, 8, 10, 4, and 11 through 13):

$$x_D = \frac{x}{L},\ t_D = \frac{1}{\phi LWH} \int_0^t q(\tau)d\tau,\ S_a = \frac{\sigma_a}{\sigma_{a0}},\ S_s = \frac{\sigma_s}{\sigma_{a0}}, C = \frac{\phi c}{\sigma_{a0}}, U_0 = \frac{q}{WH},$$
$$u = \frac{U}{U_0} = \frac{UWH}{q}, P = \frac{k_0 p}{U_0 \mu_o L} = \frac{k_0 pWH}{q\mu_o L},\ M = \frac{\mu_w}{\mu_o} \quad \cdots (B\text{-}1)$$

In dimensionless co-ordinates (Eq. B-1), the governing equations (Eqs. 7, 8, 10, 4, and 11 through 13) become

$$\nabla(u) = 0 \quad \ldots\ldots\ldots\ldots\ldots\ldots\ldots\ldots\ldots (B\text{-}2)$$

$$\frac{\partial s}{\partial t_D} + u\nabla f(s, S_s) = 0 \quad \ldots\ldots\ldots\ldots\ldots\ldots\ldots (B\text{-}3)$$

$$f(s, S_s) = \left[1 + \frac{k_{ro}(s)\mu_w(1+\beta\sigma_{a0}S_s)}{k_{rw}(s)\mu_o}\right]^{-1}$$

$$\frac{\partial}{\partial t_D}[sC + S_a + S_s] + u\nabla(Cf) = 0 \quad \ldots\ldots\ldots\ldots\ldots (B\text{-}4)$$

$$S_a = S_a(\varepsilon, s),\ \varepsilon = \varepsilon\left(\gamma, {Uf}/{s\phi}\right) \quad \ldots\ldots\ldots\ldots\ldots (B\text{-}5)$$

$$\frac{\partial S_s}{\partial t_D} = (\lambda_s L)C|u|f \quad \ldots\ldots\ldots\ldots\ldots\ldots\ldots\ldots (B\text{-}6)$$

$$\frac{\partial(\gamma s)}{\partial t_D} + u\nabla(\gamma f) = 0 \quad \ldots\ldots\ldots\ldots\ldots\ldots\ldots\ldots (B\text{-}7)$$

$$u = -\left[\frac{k_{rw}(s)}{M(1+\beta\sigma_{a0}S_s)} + k_{ro}(s)\right]\nabla P, \quad \ldots\ldots\ldots\ldots (B\text{-}8)$$

respectively.

The initial conditions corresponding to injection of low-salinity water into oil-bearing formations include initial water saturation and initial concentrations of salt and of attached particles, zero values of suspended and strained fines:

$$t_D = 0:\ s = s_{wi},\ \gamma = \gamma_i,\ S_a = 1,\ C = 0,\ S_s = 0. \quad \ldots\ldots (B\text{-}9)$$

Boundary conditions on the injection wells include rate q^j, unit fractional flow for water, salt concentration, and zero concentration of suspended fines:

$$r = r_w:\ 2\pi r k_{rwor}\frac{\partial P}{\partial r} = \frac{q^j}{q}\frac{W}{L},\quad f(1-s_{or}, 0) = 1,\ \gamma = \gamma^0,\ C = 0. \quad \ldots\ldots\ldots (B\text{-}10)$$

Well bottomhole pressure is a boundary condition at the production wells:

$$r = r_w:\ p = p^p. \quad \ldots\ldots\ldots\ldots\ldots\ldots\ldots\ldots (B\text{-}11)$$

The boundary condition on the impermeable reservoir boundaries is zero normal component of the pressure gradient.

Appendix C—Equivalence Between the Polymer-Flooding and Fines-Assisted-Waterflooding Models

In this Appendix, we map the system of fines-assisted-waterflooding on the polymer-flooding system in large-scale approximation.

Let us describe the polymer-flooding model (Lake 1989). It is assumed that oil and aqueous phases are incompressible, which leads to the volume conservation for the total two-phase flux

$$\nabla(U) = 0. \quad \ldots\ldots\ldots\ldots\ldots\ldots\ldots\ldots\ldots (C\text{-}1)$$

The volume conservation for incompressible aqueous phase, which is immiscible with oil, is

$$\phi\frac{\partial s}{\partial t} + U\nabla f(s, c_p, c_a) = 0,\ f(s, c_p, c_a) = \left[1 + \frac{k_{ro}(s)\mu_w(c_p)R_k(c_a)}{k_{rw}(s)\mu_o}\right]^{-1}. \quad \ldots\ldots\ldots (C\text{-}2)$$

The polymer concentration c is assumed to be small enough to neglect non-Newtonian properties of the polymer solution.

The polymer is present in the porous media in dissolved and adsorbed states, so the polymer mass balance is

$$\frac{\partial\left(\phi s c_p + c_a(c_p)\right)}{\partial t} + U\nabla[c_p f(s, c_p, c_a)] = 0,\ f(s, c_p, c_a) = \left[1 + \frac{k_{ro}(s)\mu_w(c_p)R_k(c_a)}{k_{rw}(s)\mu_o}\right]^{-1}. \quad \ldots\ldots\ldots (C\text{-}3)$$

Here, both dissolved and adsorbed concentrations are small if compared with the water volume and do not affect neither porosity nor volumetric balance for either phase.

The overall flux is obtained from modified Darcy's law for two-phase Newtonian flow in porous media and includes formation damage caused by adsorbed polymer:

$$U = -\left[\frac{k_{rw}(s)\,\mu_o}{\mu_w(c_p)R_k(c_a)} + k_{ro}(s)\right]\nabla p. \quad \ldots\ldots\ldots\ldots (C\text{-}4)$$

Here, the resistance factor R_k is a function of normalized adsorbed concentration:

$$R_k = 1 + (RRF - 1)\frac{c_a}{c_{a\max}} = 1 + (RRF - 1)\frac{c_a}{c_a(c_p^0)}, \quad \ldots\ldots\ldots\ldots\ldots\ldots (C\text{-}5)$$

where RRF corresponds to the maximum value of the resistance factor R_k for $c_a = c_{a\max}$.

Often the adsorption isotherm is represented in the Langmuir form:

$$c_a(c_p) = \frac{ac_p}{1+bc_p}. \quad \ldots\ldots\ldots\ldots\ldots\ldots\ldots\ldots \text{(C-6)}$$

From Eqs. C-2 and C-3, it follows that

$$\phi s\frac{\partial c_p}{\partial t} + \frac{\partial c_a(c_p)}{\partial t} + Uf\nabla[c_p] = 0. \quad \ldots\ldots\ldots\ldots\ldots \text{(C-7)}$$

The polymer-floodinging model contains sorption function $c_a = c_a\ (c_p)$, resistivity factor $R_k = R_k\ (c_a)$, and constants: Langmuir sorption constants a and b, maximum resistivity factor RRF, and injected concentration of polymers ${c_p}^0$.

Now let us map the model of the waterflood with fines on the polymer-flooding model. Polymer concentration is expressed by salt concentration as follows:

$$c_p = \frac{c_p^0}{\gamma_i - \gamma^0}(\gamma_i - \gamma). \quad \ldots\ldots\ldots\ldots\ldots\ldots\ldots\ldots \text{(C-8)}$$

This provides the initial condition for polymer concentration $c_p = 0$, where salt concentration is equal to its initial concentration $\gamma = \gamma_i$ too. Also, the inlet boundary condition for polymer $c_p = c_p^0$ corresponds to that for salt: $\gamma = \gamma^0$.

Let us propose the following expression for the polymer adsorption through the maximum retention function:

$$c_a = \frac{\delta c_p^0[\sigma_{a0} - \sigma_a(\gamma)]}{\gamma_i - \gamma^0}, \quad \ldots\ldots\ldots\ldots\ldots\ldots\ldots \text{(C-9)}$$

where $\delta \ll 1$ is a small parameter. The small parameter in Eq. C-9 is introduced to make Eq. C-7 with adsorption and Eq. B-7 without adsorption equivalent.

Substituting Eq. C-9 into Eq. C-7 yields

$$-\phi s\frac{\partial \gamma}{\partial t} + \delta\frac{\partial[\sigma_{a0} - \sigma_a(\gamma)]}{\partial t} - Uf\nabla\gamma = 0. \quad \ldots\ldots\ldots \text{(C-10)}$$

Because $\delta \ll 1$ is a small parameter, the adsorption term in Eq. C-10 can be neglected. We also assume constant viscosity of aqueous phase in Eqs. C-3 and C-4. Therefore, Eq. C-10 becomes equivalent to the salt mass balance equation (Eq. 10).

Expressing the value of the maximum resistance factor vs. the formation damage variables,

$$RRF = 1 + \beta[\sigma_{a0} - \sigma_a(\gamma^0)], \quad \ldots\ldots\ldots\ldots\ldots\ldots \text{(C-11)}$$

yields

$$\begin{aligned} R_k &= 1 + (RRF - 1)\frac{c_a}{c_a(c_p^0)} \quad \ldots\ldots\ldots\ldots\ldots \text{(C-12)} \\ &= 1 + \beta[\sigma_{a0} - \sigma_a(\gamma)], \end{aligned}$$

so the equations for the total two-phase flux for polymer (Eqs. C-4 and C-5) and fines (Eq. 19) become equivalent.

Finally, the system of equations for two-phase flow with varying water salinity and fines mobilization can be "translated" into the polymer-flooding model with the "dictionary" given by the formulae in Eqs. C-8 through C-11.

From Eqs. C-8 and C-9 follows the expression for polymer adsorption isotherm for the "fines-substituting" polymer:

$$c_a = \frac{\delta c_p^0\left[\sigma_{a0} - \sigma_a\left(\gamma_i - \dfrac{c_p^0(\gamma_i - \gamma^0)}{c_p^0}, s\right)\right]}{\gamma_i - \gamma^0}. \quad \ldots\ldots\ldots \text{(C-13)}$$

It is assumed that salinity variation and fines mobilization do not change viscosity of water. Therefore, polymer viscosity in Eq. C-4 is

$$\mu_w(c_p) = \mu_w(0). \quad \ldots\ldots\ldots\ldots\ldots\ldots\ldots\ldots \text{(C-14)}$$

If the initial concentration of attached fines is less than that corresponding to the initial salt concentration (i.e., if the initial salt concentration is higher than the critical initial salt concentration for the reservoir fines), the flood process is described by the system in Eqs. 16 through 18 only for salt concentrations below the critical value. Flow with salt concentrations above the critical value is described by the damage-free system of two-phase flow in porous media (black-oil model).

Abbas Zeinijahromi is presently lecturer in Petroleum Engineering at the Australian School of Petroleum at the University of Adelaide, carrying out theoretical work, experimental studies, and reservoir simulation of formation damage and IOR. e-mail: abbas.zeinijahromi@adelaide.edu.au. He holds a BSc degree in production engineering and PhD and MSc degrees in reservoir engineering.

Thi K.P. Nguyen joined Santos Ltd. as a reservoir engineer in 2012. She holds a BS degree in petroleum and chemical engineering and an MS degree in petroleum engineering from Adelaide University.

Pavel Bedrikovetsky is an author of two books in reservoir engineering and 150 technical papers in international journals. e-mail: pavel@asp.adelaide.edu.au. His research covers formation damage and IOR. From 1991–1994 he was a Visiting Professor at Delft University of Technology and at Imperial College of Science and Technology. Since 1994, he is a Petrobras Staff Consultant. Currently he holds a Chair in petroleum engineering at the University of Adelaide. He holds an MSc degree in applied mathematics, a PhD degree in fluid mechanics, and a DSc degree in reservoir engineering from Moscow Oil-Gas Gubkin University. He has served as Section chairman, a short-course instructor, a key speaker and Steering Committee member at several SPE conferences. He was also a 2008–2009 SPE Distinguished Lecturer.